Trapping Cold Rubidium in a Fiber

by

David Ross Brown

Submitted to the Department of Physics
in partial fulfillment of the requirements for the degree of

Bachelor of Science in Physics

at the

MASSACHUSETTS INSTITUTE OF TECHNOLOGY

June 2007

Author .....
Department of Physics
May 11, 2007

Certified by .....
Professor Vladan Vuletić
Lester Wolfe Associate Professor of Physics
Thesis Supervisor

Accepted by .....
Professor David R. Pritchard
Cecil and Ida Green Professor of Physics
Senior Thesis Coordinator, Department of Physics

Trapping Cold Rubidium in a Fiber

by

David Ross Brown

Submitted to the Department of Physics
on May 11, 2007, in partial fulfillment of the
requirements for the degree of
Bachelor of Science in Physics

Abstract

In this thesis, we demonstrate the novel technique of loading cold ^{87}Rb into a red-detuned optical dipole trap within a hollow core photonic fiber. This confines the atoms to 6 microns in two dimensions. We initially cooled the Rubidium in a magneto-optical trap. The great confinement of the Rubidium allows for increased optical depths per atom and therefore increased interaction rates with probing light.

Thesis Supervisor: Professor Vladan Vuletić
Title: Lester Wolfe Associate Professor of Physics

Acknowledgments

This project and this paper could not have happened without the help of a lot of people. First of all, Dr. Vlatko Balic and graduate student Misho Bajcsy worked tirelessly on this experiment. They were always there when I had questions about the experiment and about my project. While I have held sway over the northwest corner of the room Yiwen Chu, another undergraduate, has held the southwest. She was particularly helpful when I was writing my thesis, and I am sure she will be successful at Harvard.

Before I worked on this project, I worked on the ion trap experiment of Andrew Grier and Marko Cetina. At the time John Campbell, who has since moved on to West Point, was working in the lab. Over the year I worked with them I learned the basic skills of machining, soldering and design that made me useful in Vlatko's laboratory.

I couldn't be here without Vladan. When my UROP fell through at the last minute sophomore year, it was Vladan that came through and gave me a job when I thought all was lost. He is a talented researcher and a great educator. In addition he is now a tenured faculty member and a proud father, for which I congratulate him.

I'd like to thank David Pritchard for funding me over the last summer out of his own funds when Vladan's fund fell through.

And of course there are all the many people in my life who have made this possible. My junior lab partner, Tucker Jones, with whom I will be spending the next five years at Caltech, has been my constant foil in my four year struggle against the fell forces of the Institute. My housemates have been supportive of me in times of need, and tolerant of me when I was stressed out and taking it out on them.

Finally, I'd like to thank my mother and father. They paid for my education. They pushed me towards success. They supported my career in science. Thanks mom. Thanks dad. This ones for you.

Contents

List of Figures

List of Tables

Chapter 1

Introduction

One of the prominent challenges that faces modern atomic physics is the problem of quantum computation. Though great strides have been made in this field with NMR based quantum computers, this approach has been stymied by the statistics of large numbers of atoms. The question then becomes how to make a scalably large quantum computer. One answer to this question being vigorously researched is the implementation of an optical quantum computer. This would be a quantum computer in which the qubits have as their basis the magnetic substates of the photon. This approach is advantageous in the relative ease of maintaining the coherence of the quantum state of the light. Its disadvantage is the difficulty inherent in single photon interactions: the problems of single photon creation, storage and manipulation. The question that this experiment deals with is that of single photon manipulation.

One goal of photon manipulation is to make a quantum interference gate that changes the phase of a photon. Ideally this gate would

have as its control signal a single photon. This sort of concept has been demonstrated using EIT with a 23 photon control signal[2]. Trapping within a fiber will increase the optical depth per photon so that such a gate would be realizable. If this gate was actually realized it would have applications not only to quantum computation but also to communications. It would represent an ultrafast, low power switching mechanism.

1.1 Trapping within a Fiber

The reason we are trapping inside a photonic fiber is that this traps the rubidium very tightly and confines the light we probe it with into the same region. In this situation one finds that the optical depth[1] goes as the inverse of the confinement area. This holds out the possibility that for great enough confinement very few atoms can be used to create large optical depths, thereby increasing the photon-atom interaction rate.

1.2 Outline of Thesis

The focus of this thesis is on the interaction between the lasers and the elements of the experiments with a strong emphasis on the technical details of our setup. In chapter 2 I will give a general overview of the experiment and apparatus. In chapter 3 I will go into technical detail about our lasers and the manner in which we lock them to the spectral

[1]Optical depth is a measurement of the opacity of a substance to light.

lines of rubidium. In chapter 4 I will discuss the MOT and optical pumping. In chapter 5 I will discuss the optical dipole trap. Chapter 6 will be a discussion of the results of the experiment.

Chapter 2

Experimental Overview

An image of the central chamber of our apparatus can be seen in figure 2-1. Our apparatus is a vacuum chamber pumped down to a pressure of around 2×10^{-9} torr. The central component of our vacuum chamber is surrounded by anti-Helmholtz coils which produce a magnetic field gradient of ≈ 4.2 gauss/(cm $\cdot$ A) along the major axis and ≈ 2.1 gauss/(cm $\cdot$ A) along the minor axes. Our experiment uses this quadrupole magnetic field and lasers aligned to the D2 transition of ^{87}Rb. An 80 mW laser beam is split in three portions to provide the trapping beam for the MOT. A 12 mW laser is split in three portions to provide the repump beam of the lock. We lock our lasers in a two step method. Our reference lasers are locked using the Saturation DAVLL[12][17] technique onto a transition in ^{85}Rb. We then use the data in appendix A to determine the frequency shift between the lock frequency and the desired frequency in our other lasers. A comparator and a PLL are used to lock these lasers onto this frequency difference.

Our source of Rb is an SAES alkali metal getter. This is a wire

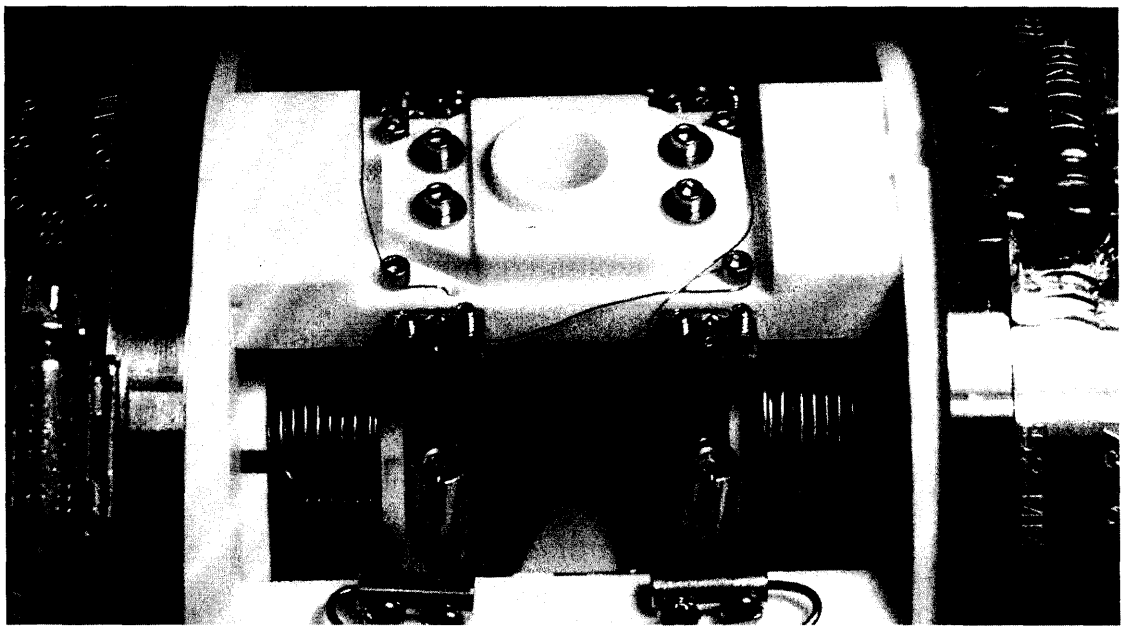

Figure 2-1: Central Chamber of the Apparatus
The quadrupole funnel trap is clearly visible emanating from the top of the chuck that holds the optical fiber. The main axis anti-Helmholtz coils are clearly visible. The Rubidium getters are not visible, but the wires that contact them are visible directly to the left and right of the anti-Helmholtz coils.

that runs into our vacuum chamber that is coated with RbCl. We put 4.5 Amperes through this wire to put this Rb into the trap. We then perform the following process:

- t=0

  Current=3A

  Laser Detuning: 20 MHz

  MOT Cooling

- t=800 ms

  Current=12A

  Compression

- t=820 ms

  Laser Detuning: 140 MHz

- t=850 ms

  Current=0 A

  Polarization Gradient Cooling

- t=865 ms

  Turn off MOT Laser. Turn on D1 Laser

  Optical Pumping

- t=865.5 ms

  Current = 18A

  Turn on quadrupole funnel trap

  We allow the distribution to thermalize

- t=885.5 ms

  We move the atom cloud down the quadrupole funnel trap

- t=915.5 ms

  Load atoms into a hollow core optical fiber. Perform experiment.

Most of the stages will be discussed in greater detail below. Polarization gradient cooling, due to the complexity of the subject and the space limitations of the paper, will not be discussed. For more detailed information on the subject see[6][7][16].

The goal of the experiment is to trap the atoms tightly in our hollow core fiber using an optical dipole. This fiber is HC-800-02 hollow core fiber made by Crystal Fibre. Our optical dipole trap uses a diode laser at 784 nm. The dipole laser is therefore blue-detuned from the 795 nm D1 transition in ^{87}Rb and red-detuned from the 780 nm D2 transition in ^{87}Rb.

Chapter 3

Laser Locks

The primary working element of an atomic physics experiment is the laser, which by tuning to frequencies relative to transitions in atomic species can manipulate those species. But the commercial lasers we use are not internally frequency stable. They can mode-hop and they can shift in frequency due to the effects of external noise such as pick-up on the wire and mechanical vibrations of the optics table. We therefore need to frequency stabilize them with a linear feedback circuit. This requires a method of generating a linear signal that indicates the error of the laser's frequency relative to the actual frequency and control circuitry.

3.1 PI Control Board

We use a PI circuit to control the frequency of the laser based on the error signal. See figure 3-1 for a schematic of this board. See appendix B for the detailed schematic (figure B-1) and layout (figure B-2) of the

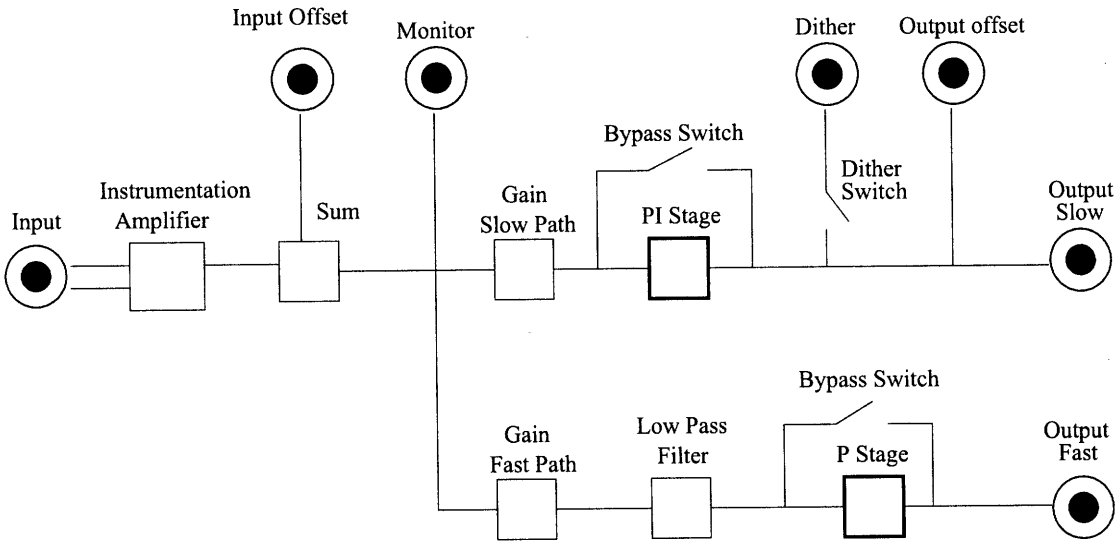

Figure 3-1: Schematic of the PI Control Board
Note there are two pathways for feedback in this board. We can control input and output offset to the board with potentiometers. We also have control on the gain of the feedback stages. The circles are external connections.

board.

A PI circuit is a circuit with both proportional and integral gain. Proportional gain is used to compensate for errors. If the system gets an input signal of a relative to the zero-point of the laser lock, the proportional stage will output $P \times a$, where P is the proportional gain, which we can set with a pair of potentiometers. Integral gain similarly outputs a signal $\int dtI \times a$, where I is the integral gain. The integral gain then serves to stabilize the lock around the zero error point. Proportional gain alone leads to a steady-state error in the output. On the other hand too large a portion of integral gain means that the system is slower to compensate for errors.

In order to phase lock a signal, it is essential that the phase shift around the closed path not be 180° at any frequency that has unity gain.

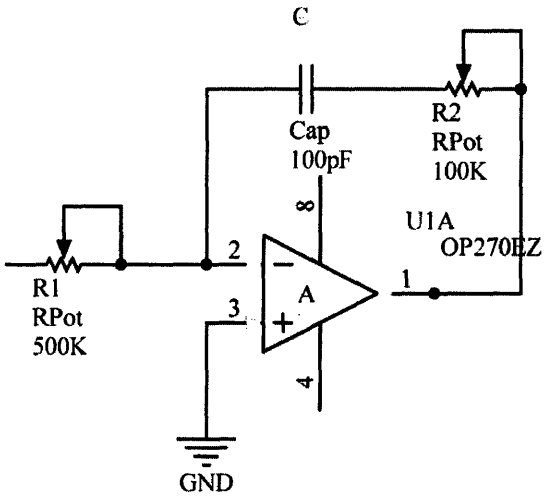

Figure 3-2: Schematic of the PI Element
This element is the PI stage in out box. The proportional gain is set by R_1 and R_2. The integral gain is set by C and R_1.

Otherwise we would expect self-oscillation at that frequency, which would severely disrupt the laser. In the language of control theory, we want a good phase margin: the difference from a 180° of the phase shift at unity gain. To assure that our system will lock to the correct frequency we require that the Nyquist stability criteria hold. As a rule of thumb, this means that the point of 45° phase shift have a gain of one half.[8] For the PI controller this is very simple to do. The PI itself has a transfer function, $H(\omega)$ which produces a gain:

$$\frac{V_{out}}{V_{in}} = \frac{1}{\omega C R_1}\left(1 + R_2^2\omega^2 C^2\right)^{\frac{1}{2}} \tag{3.1}$$

and phase-shift

$$\phi = \arctan \frac{1}{R_2 \omega C} \tag{3.2}$$

Where R_1, R_2 and C are the resistances and capacitance as seen in figure 3-2. As we can alter the overall gain to the PI stage through an independent pre-factor, keeping to the Nyquist stability criteria is not difficult. However the other components of our boards provide additional phase shift at higher frequency. The reason is that the op-amps we use are not ideal, and so their gain falls at higher frequencies which implies a phase shift in this frequency. Even after the board was optimized, there was still a phase-shift of 26° at 100 KHz as seen in figure 3-3a. This means that the lock board can only compensate for noise in frequencies lower than this cutoff. Below this cutoff we can select a limiting point at which to put the knee of our PI controller. Beyond the knee the integral gain falls off at 20 dB per decade, so that the smaller proportional gain dominates.

The PI board in closed loop mode behaves as expected. Let us call the gain in open loop mood, $H(\omega)$, which for our PI board is equation 3.1. The close loop gain is:

$$F(\omega) = \frac{H(\omega)}{1 + G(\omega)} \tag{3.3}$$

Where $G(\omega)$ is the transfer function of the entire loop. When we tested the closed-loop gain of the PI board, we found that $H(\omega) = G(\omega)$. At

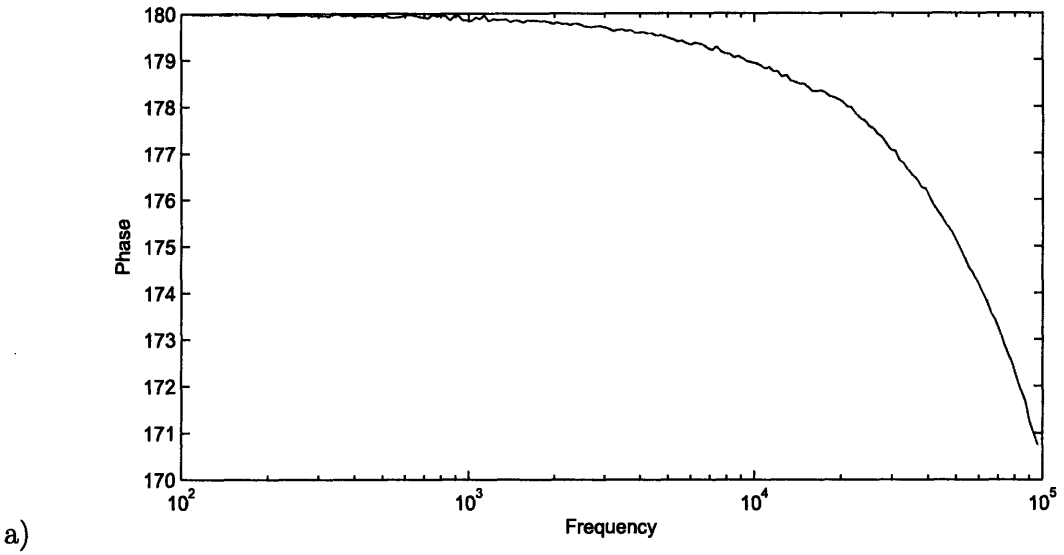

a)

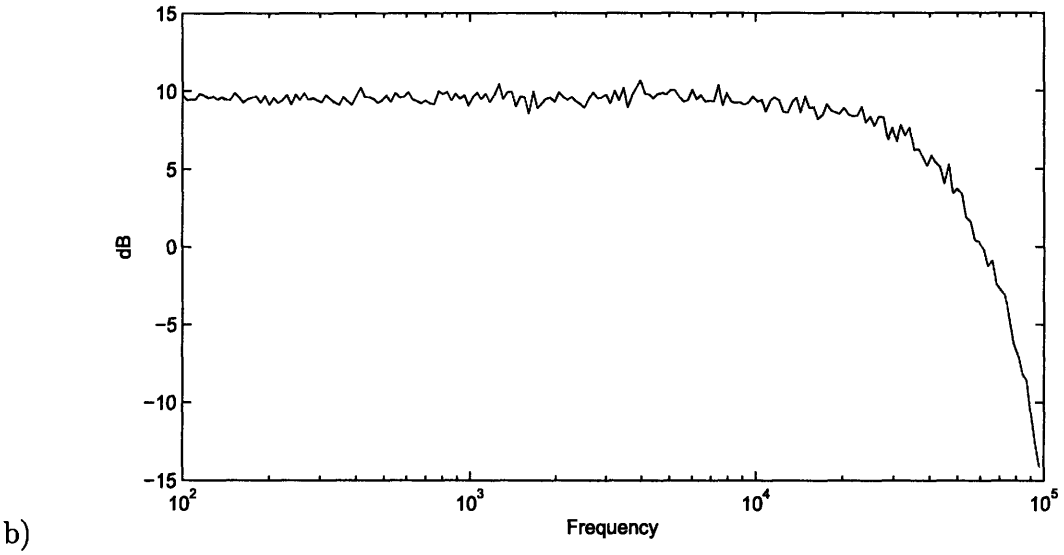

b)

Figure 3-3: Transfer Function and Phase Responses of Various Elements
The x-axis in all of these graphs is frequency in Hertz. a) Shows the phase change with increasing frequency due solely to the non-ideal op-amps in the PI controller board. The y-axis is phase shift. b) Shows the closed loop gain of the PI controller with the 3 dB point set to 35 KHz.

low frequency we expect that:

$$F(\omega) = \frac{\omega R_1 C}{1 + \omega R_1 C} \tag{3.4}$$

and at high frequency, it should be a constant determined by the proportional gain. Between the two regimes the closed loop gain should change at 20 dB per decade. Figure 3-3b, which displays the close loop gain versus frequency confirms this interpretation.

Some of our lasers had two feedback inputs, typically a piezo-electric control and a current control. The former is better suited for lower frequency operation and the latter for higher frequency operation. Accordingly we would set the knee on the piezo control to less than 1 KHz with very little proportional gain. The current path was preceded by a 10 KHz high pass filter in order that there not be cross-talk between the two paths at low frequencies.

The current path has only a proportional gain stage. This was necessary because the gain of the high pass filter cancelled with the gain of the integrator at low frequencies; we found cross-talk between the two feedback paths. An integrator acts to decrease gain beyond the 3 dB point by 20 dB per decade. A first order low pass filter increases the gain beyond the 3 dB point by 20 dB per decade. Clearly these would come into conflict at some intermediate frequency. In order to avoid cross-talk and keep the integral gain, we would need a higher order filter. We decided that this would not be worth the effort.

Fortunately, the integral gain is not strictly necessary at higher fre-

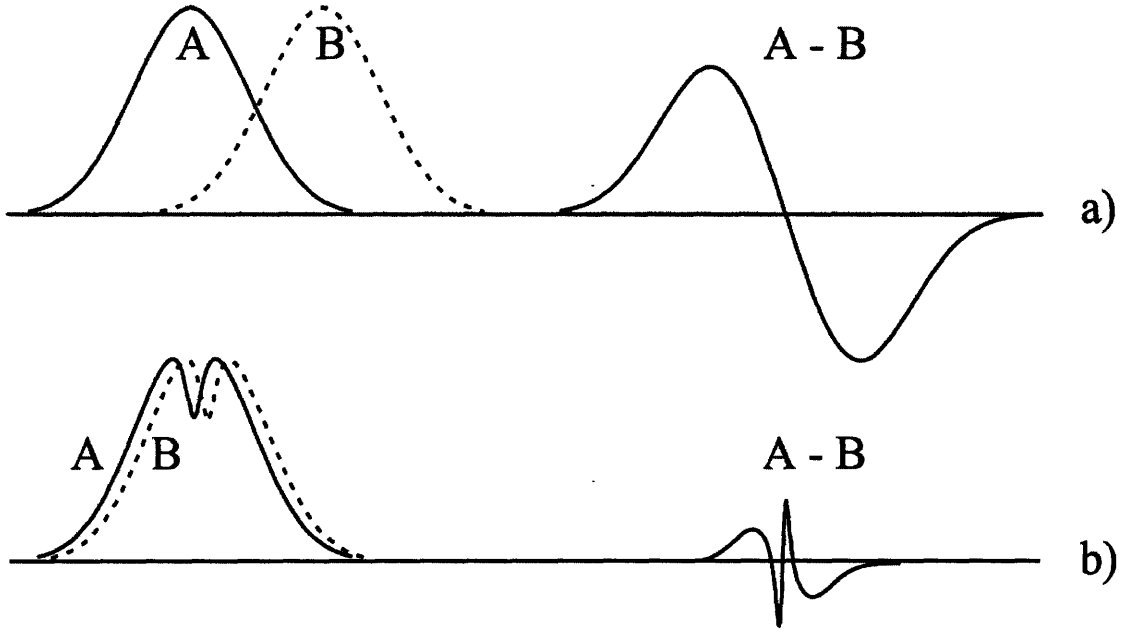

Figure 3-4: Lineshapes for DAVLL and Saturated DAVLL
a) Shows the lineshapes associated with σ^+ and σ^- light and their associated subtracted signal for a DAVLL. The linear slope at the zero crossing corresponds to the resonant frequency.
b) Shows the lineshapes associated with a saturated absorption DAVLL as we use in our experiment. Note the extremely sharp slope at the zero-crossing and the small magnetic field needed to exact that slope. Image is copyright to Petelski et al.[12]

quencies. Proportional gain alone leads to a problem in which the system settles at the wrong value. As the high frequency path does not deal with such DC offsets, it proves acceptable to use only proportional gain in the current path.

You might also expect that there would be also cross-talk at high frequencies. There is not because the transfer function of the piezo is zero at those frequencies.

3.2 Saturation DAVLL Locked Lasers

In order to lock our master lasers to the preferred frequencies we use Saturation Absorption DAVLL which is the synthesis of the technique of Doppler free saturation absorption spectroscopy and Dichroic Atomic Vapor Laser Lock (DAVLL) techniques.

3.2.1 DAVLL

DAVLL locks were conceived in the 1998 as a cheaper method of locking lasers that did not require direct modulation of the lasers[5]. In this method a linear polarized laser beam is shined through a vapor cell containing the atomic species. The vapor cell is a tube wrapped in coils. When current runs through the coils, the cell is heated up and the atoms vaporize. A magnetic field is directed along the axis of laser propagation. The light emitted from the vapor cell is then sent through a beam-splitter. As linearly polarized light can be viewed as a super-position of σ^+ and σ^- light, the beam splitter splits these two components of the light which enter two separate photo-detectors. The signal from the σ^+ light is then separated from the signal of the σ^- light. Due to the Zeeman effect the emission spectrum of the rubidium in the vapor cell is split (see figure 3-4a). Therefore when the two spectrum are subtracted from each other the resultant spectrum has two useful properties: the point of maximum slope of the subtracted signal is the frequency of the transition in rubidium, and about that point the signal is very linear. This allows for it to produce a useful

error signal.

3.2.2 Saturation Absorption Spectroscopy

Suppose one has a cloud of rubidium at a given temperature T with a transition at frequency ν_0. One would expect that it would have a Gaussian absorption lineshape whose standard deviation was dictated primarily by it's temperature. That is to say that at some $\nu = \nu_0 + \delta$ you would expect absorption of those atoms with velocity v such that $\delta = -\nu_0 \frac{v}{c}$ due to the Doppler shifting of the atoms at that velocity. It is then clear that the DAVLL lock is limited by the Doppler broadening of the lineshapes of rubidium. A thinner lineshape would result in a larger slope and therefore a better lock.

One way to get around this Doppler limitation is through saturation spectroscopy. If one were to look at the velocity distribution of the absorbers one would normally discover that they were distribute in a Gaussian pattern about $v = 0$ with a standard deviation determined by their temperature. However this depends on most of the atoms being in the ground state of the transition in question. If you were to selectively depopulate atoms at a given velocity then there would be a hole in the velocity distribution. Indeed this can be done by taking a laser with line width much smaller than the standard deviation of the Gaussian lineshape and shining it at the atoms. A hole is 'burnt" in the velocity distribution of absorbers; a significant portion of the absorbers are now in the excited state and therefore dark to laser probing.

Consider a group of atoms moving at v, and a laser of frequency ν. The pump beam will only excite these atoms if $\nu + \Delta\nu$ corresponds roughly to a hyperfine transition of rubidium. Then if we shine a counter-propagating probe laser of low intensity at those same atoms we should expect to detect the hole in the velocity distribution if $\nu - \Delta\nu$ also corresponds to a hyperfine transition. In this case we would see a hole in the absorption spectrum of the rubidium, commonly called the Lamb dip as seen in figure 3-4b.

3.2.3 Saturation Absorption DAVLL

Now if we do saturation absorption spectroscopy under a magnetic field that causes a Zeeman shift we should expect there to be two different absorption spectrums for σ^+ and σ^- light. Subtracting these two spectrum from one another and we should receive a signal as in figure 3-4b. This has an extremely sharp slope centered at the transition frequencies that we can use to make the error signal for our laser lock.[12]

3.2.4 Technical Information on our Reference Lasers

We use two reference lasers in our experiment. One of these is set to the D1 line of Rubidium and the other is set to the D2 line. We lock our reference lasers onto cross-over peaks in ^{85}Rb, though we carry out our experiment on ^{87}Rb because ^{85}Rb has stronger lines on which to lock our lasers. For our lock lasers we use a low power Extended Cavity Diode Laser locked to the (F=3 to F'=2/3) D1 crossover resonance. For our

D2 line we use a TEC 50 DFB laser produced by Sacher Lasertechnik. It has a default wavelength of 780.2 nm. We lock this laser onto the (F=3 to F'=3/4) crossover resonance. Frequency resolution of these transitions can be found in Appendix A.

Figure 3-5 shows a schematic of optical path that our master lasers take. After leaving the laser, the light goes through an optical isolator which attenuates reflected light by 30 dB. A waveplate that can be adjusted between 0 and $\lambda/2$ is used in combination with a polarizing beamsplitter to adjust the relative amount of light that goes down either optics pathway. One pathway attenuates the signal into an optical fiber. The other pathway puts the light into the Rubidium vapor cell for the Saturated DAVLL. The Rubidium vapor cell is a glass tube wrapped in a coil. The coil is used to produce the axial magnetic field needed to Zeeman split the transitions, but has the side effect of heating the Rubidium by two to three degrees Centigrade. This causes temperature differentials within the cell. In particular the axially aligned windows of the cell are relatively cold; over time they accumulate deposits of Rubidium which diminishes the optical depth. Therefore every two months we need to clean out the vapor cell because the lock signal is too small.

After heading through the cell the light's polarization is rotated by a quarter waveplate. A polarizing beamsplitter serves to split the light into σ^+ and σ^- light. The balanced photodetector subtracts the two signals, which are Zeeman split from one another. This is fed into the

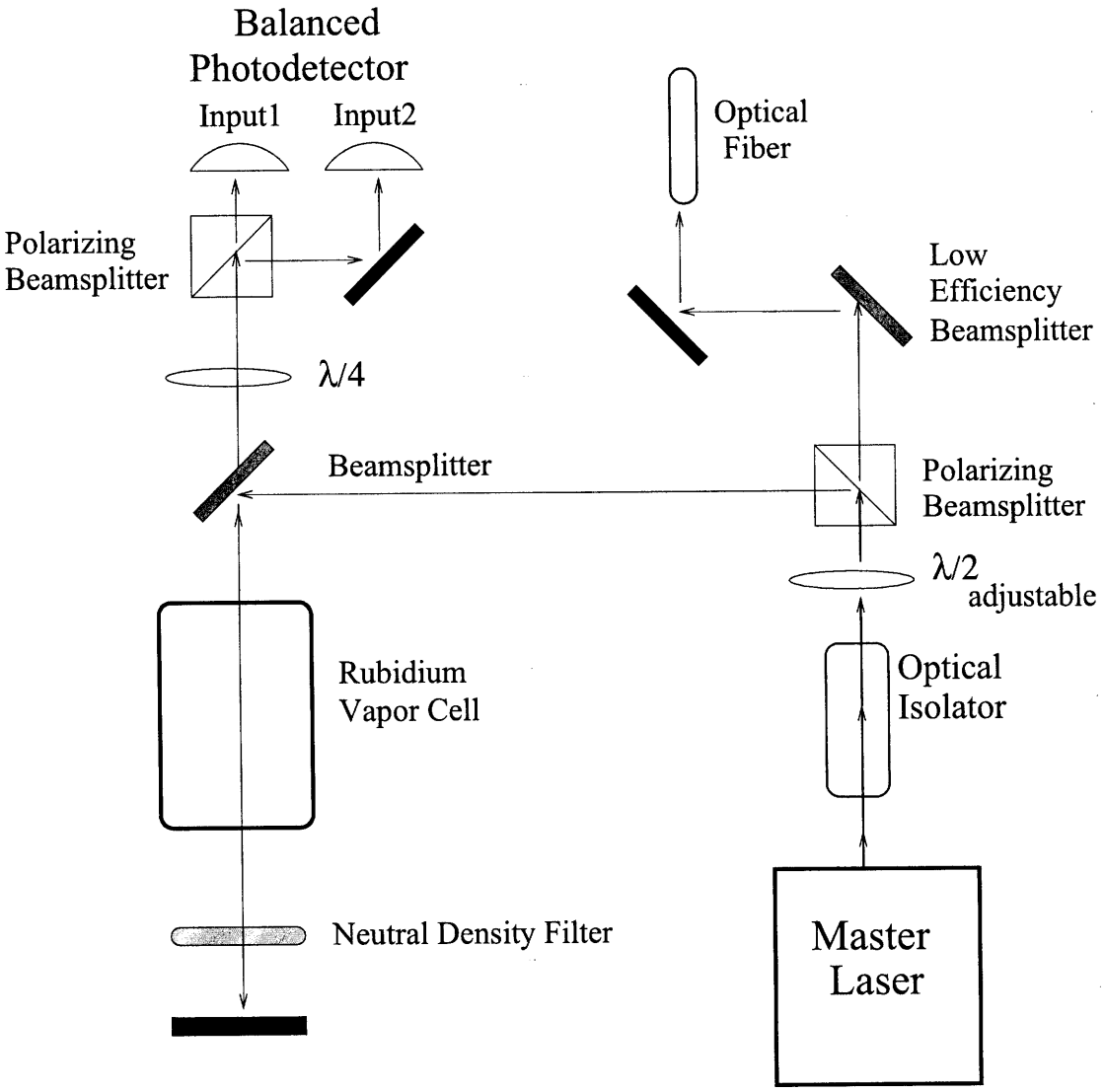

Figure 3-5: Schematic of Reference Laser Optical Path

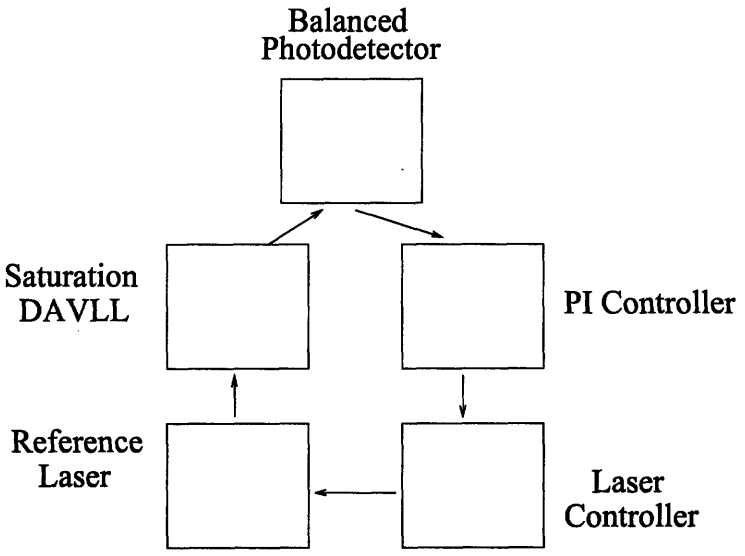

Figure 3-6: Control Path of Master Laser Lock

input of the PI controller board.

The PI controller adjusts the laser controller which tunes the laser and completes the feedback loop. We typically dither the laser to determine where the transition we want to lock onto is located. We sometimes find that this transition drifts slightly from day to day due to laser and electronics drift. Figure 3-7 shows the spectrum analyzer data for one of our beat-note PLL locks. The spectrum analyzer records the amount of noise at each frequency, from zero to 100 KHz, that the lock sees at its error output and is therefore a good way of determining the effectiveness of the lock.

3.3 Phase Lock Loop Controlled Lasers

In order to lock the slave lasers onto the desired frequency we take advantage of the fact that the difference between transition frequencies

Figure 3-7: Beat note from a Lock
The y axis is logarithmic at 10 dB/M. The large peak in the center represents the frequency difference we are locking on to. The width of this line, $\approx$ 5 MHz, is the FWHM of the laser. Every horizontal box is 200 MHz. The second peak on the right side of the image is a second mode or resonance of the beat note. Its frequency is twice that of the large peak.

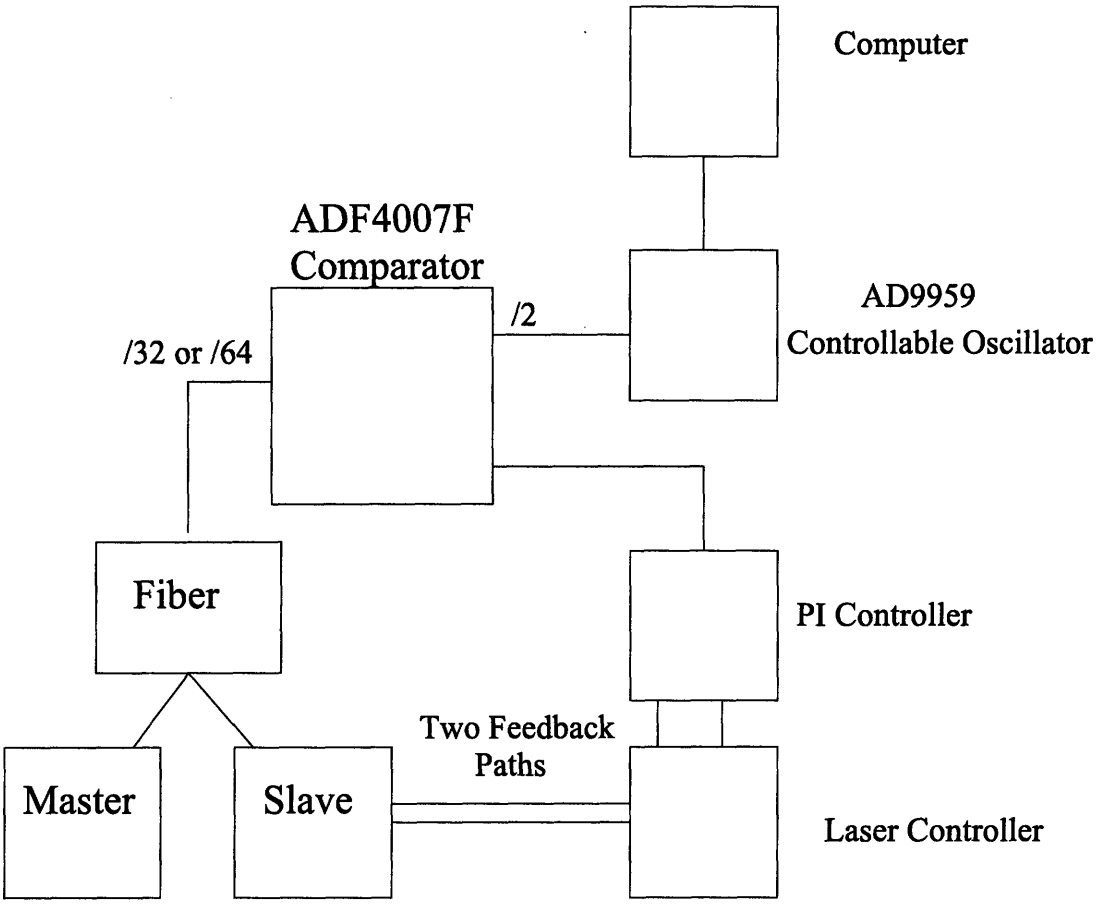

Figure 3-8: Feedback Path for the Slave Lasers

in rubidium are very well documented.[15][1] Our method locks the laser on to the desired frequency difference. Figure 3-8 is a schematic of the phase loop we use to do so.

The master and slave laser both enter the same optical fiber. The field in the fiber is:

$$E_{tot}^2 = (E_1 + E_2)^2 \tag{3.5}$$

The electric field has multiple components which have different characteristic frequencies. However, the component of the form $Ae^{i(\omega_1 - \omega_2)}$ is at far lower frequency then any of the other components of the field.

As we input this signal into electronics, these higher frequency components average to zero when read by the photodetector We input this signal into an ADF4007F comparator where it is divided by 64 or 32. It is compared with the signal from an AD9959 controllable oscillator divided by 2. The AD9959 receives its input signal in turn from a computer program. The comparison of the frequency difference between these two signals charges a capacitor which in turn produces a voltage. The voltage output is determined by a loop-filter that we had soldered onto the ADF4007F with a frequency bandwidth of five hundred kilohertz. This outputs to the PI controller which controls the laser controller and slave laser as outlined in previous sections. When the laser is locked the monitor output on the PI controller shows a signal that rapidly oscillates between a positive value and a negative value.

3.3.1 Technical Implementation

We have several lasers that we use as slave lasers. There are three tuned on or near D2 transitions of ^{87}Rb and one tuned to a D1 transition of ^{87}Rb.

Figure 3-9 is a schematic of the optical path taken by our slave laser. In order to utilize the beat note we put both slave and master laser into the same fiber. The slave laser is sent through a waveplate that is adjustable up to $\lambda/2$ and then reflected into a polarizing beamsplitter to adjust the amount of light that goes into down either path. The

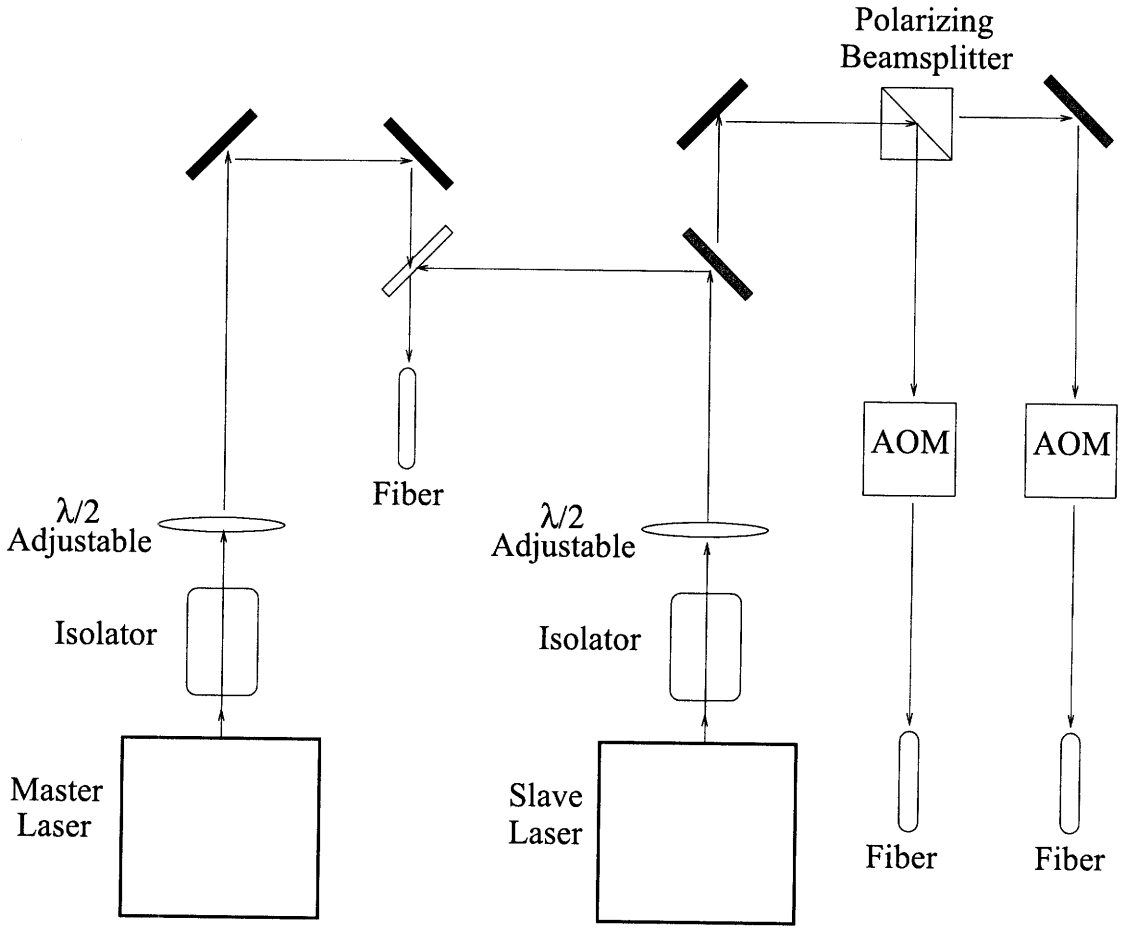

Figure 3-9: Optics Path of the Slave Laser

laser also goes through an AOM, which we use to shutter the lasers. The fibers are so arranged that if the AOM is turned on, the portion of the beam diffracted by the AOM enters the fiber.

Chapter 4

The Magneto-Optical Trap and Optical Pumping

4.1 Magneto-Optical Trap Theory and Overview

The magneto-optical trap has, since its inception twenty years ago[14], become one of the primary workhorses of atomic physics. It provides a simple and reliable way in which to trap and cool neutral atoms.

4.1.1 Laser Cooling

The lasers in the magneto-optical trap act to cool the atom. To do this we must detune the laser by some frequency δ from an atomic transition in the Rubidium. Our detuning cannot be large: the absorption spectrum for a transition falls off with δ as approximately $\frac{1}{\delta^2}$.[4] Thus if we were to far-detune the light we would have little interaction with the atom and would not expect there to be much cooling. In detuning our laser we should *red-detune* it; that is to say that the laser light should

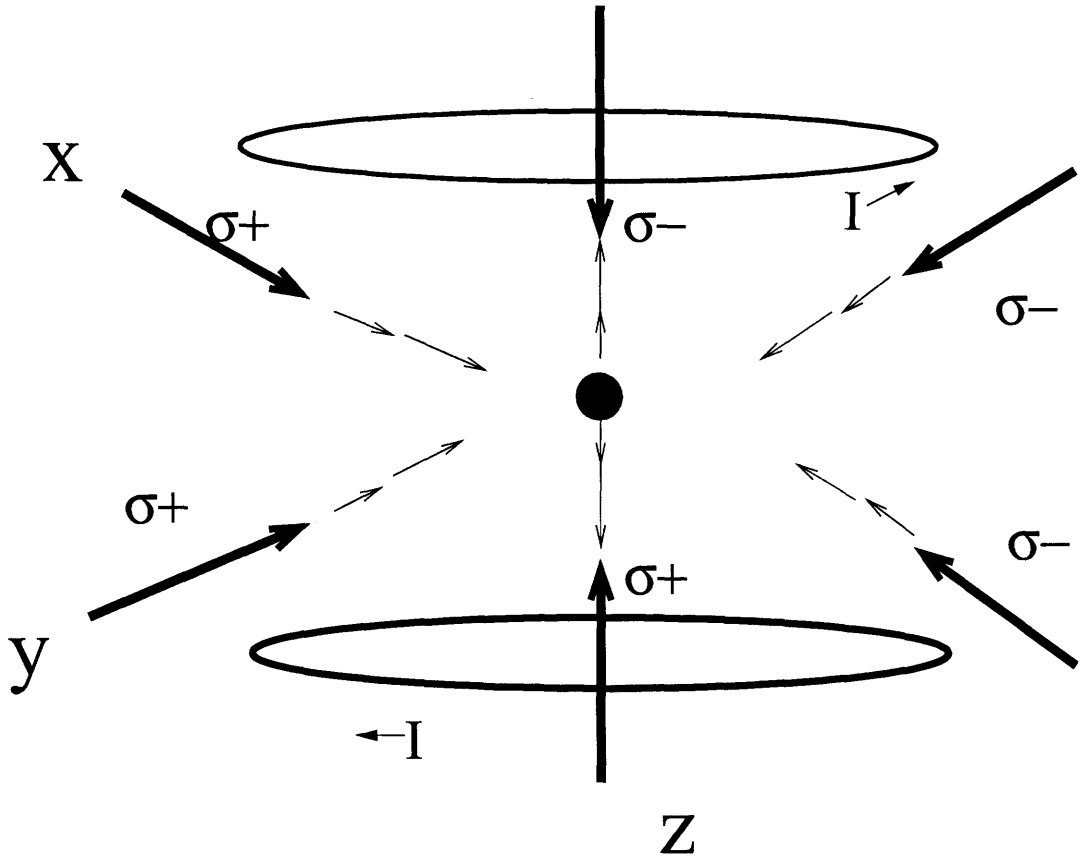

Figure 4-1: A Schematic of a Magneto-Optical Trap
The circles represent the anti-Helmholtz coils that present a quadrupole magnetic field. The thin lines are the directions of the magnetic field. The thick lines are the direction of propagation of each beam of laser light. Each laser beam is labeled with its polarization.

be red-shifted, or at lower frequency, than the atomic transition.

Consider an atom interacting with and absorbing a photon coming from the $\hat{x}$ direction. One would expect that this would impart some momentum to the atom in that $\hat{x}$ direction. When the atoms emits spontaneously it will do so without regard to direction. Therefore over an ensemble of the atoms, the atom will be pushed in the direction of the beam. The force on the atom will be determined by $\vec{F} = \gamma_s \hbar \vec{k}$, where γ_s is the scattering rate. This scattering rate is:

$$\vec{\gamma_s} = \frac{\gamma}{2} \frac{s_0}{(1 + s_0 + (2\delta/\gamma)^2} \tag{4.1}$$

Where $s_0 = I/I_{sat}$ is the saturation parameter. Let us go to the case of low intensity($s_0 << 1$) and assume that the atom has some velocity v. Let us then shine two counter-propagating beams of light at the atom. The resultant force would be:

$$F(v) = \hbar k \frac{\gamma}{2} \frac{s_0}{1 + \left[\frac{2(\delta - kv)}{\gamma}\right]^2} - \hbar k \frac{\gamma}{2} \frac{s_0}{1 + \left[\frac{2(\delta + kv)}{\gamma}\right]^2} \tag{4.2}$$

We can simplify this for clarity in the case of small v, which is accurate at low temperature to:

$$F(v) = 8\hbar k^2 \frac{\delta}{\gamma} \frac{s_0}{\left(1 + \left(\frac{2\delta}{\gamma}\right)^2\right)^2} v = -Av \tag{4.3}$$

This presents the force from the two beams as that of a drag force. It should be clear that only if $\delta < 0$, or red-detuned, does this process

serve to resist the velocity of the atoms and thereby cool them.[13] There is a natural limit to this cooling due to the thermodynamic equilibrium between the laser cooling and heating due to diffusion of the ensemble. This associated temperature is the Doppler temperature:

$$k_B T_{Doppler} = \frac{1}{2}\hbar\gamma \tag{4.4}$$

and is about $140\mu K$ for Rubidium.[15]

This method can cause cooling, but it cannot be used to trap atoms in three dimensions. By trapping in one dimension this way we cause increased expansion of the atomic cloud in the other two dimensions, so that if we were to similarly try to trap in those two directions the net force on the atoms would be zero. This phenomenon is known as the Optical Earnshaw Theorem. To overcome this limitation non-optical forces are required.

4.1.2 Zeeman Effect

In order to overcome the limitations of the Optical Earnshaw Theorem, we introduce a magnetic field on the trap through anti-Helmholtz coils, which provide a magnetic field of intensity:

$$B = A\sqrt{x^2 + y^2 + 4z^2} \tag{4.5}$$

With direction relative to the trap center indicated as in figure 4-1.

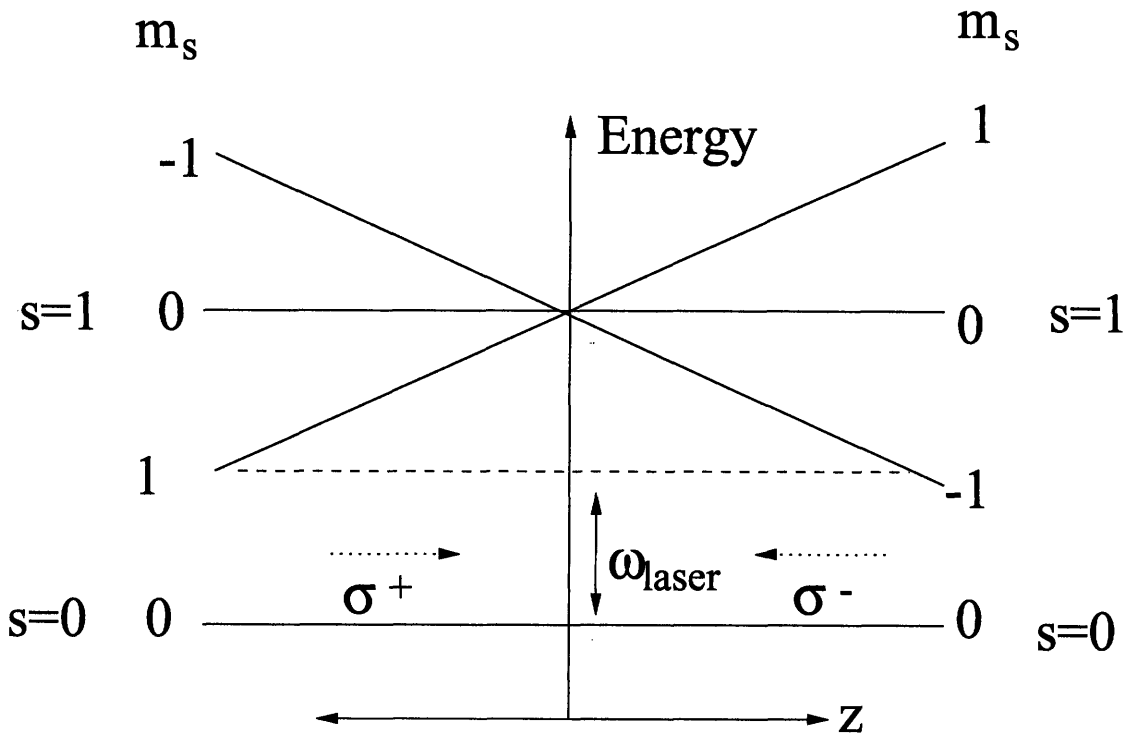

Figure 4-2: Energy Levels in the MOT
For $z > 0$, the σ^- transition is closer to resonance, and for $z < 0$ the σ^+ transition is closer to resonance.

This Zeeman splits the transitions to $m = 1$ and to $m = -1$ by $\mu' Bm$, where B is the magnetic field, m is the magnetic quantum number and μ' is the effective magneton for the particular system. This splits the transitions as shown in figure 4-2. If you then beam σ^+ light, which stimulates $m = 0 \rightarrow m = 1$, from $-\hat{z}$ and σ^- light, which stimulates $m = 0 \rightarrow m = -1$ from $\hat{z}$ you will find that for $z > 0$ the ensemble will absorb more σ^- than σ^+ and thus be restored toward $z = 0$. Similarly for $z < 0$ more σ^+ than σ^- will be absorbed and the ensemble becomes trapped near $z = 0$.

Given an atom at some position z, the effective detuning from the transition will be $\delta_\pm = \delta \mp \vec{k} \cdot \vec{v} \pm \mu' B(z)/\hbar$, where $+$ and $-$ determine

which polarization of light is being considered. Note that this contains a term that represents the Doppler shift and a term that represents the Zeeman shift and that the signs of these two terms are inextricably linked. We would then expect there to be a force on the atoms $\vec{F} = \vec{F_+} + \vec{F_-}$, where:[13]

$$\vec{F\pm} = \pm\hbar\vec{k}\gamma_s(\delta_\pm) \tag{4.6}$$

This method of cooling can easily be extended to the three dimensional case. As we use anti-Helmholtz coils to create a quadrupole field, there is also a magnetic field gradient in the $\hat{y}$ and $\hat{z}$ directions as in figure 4-4. In the $\hat{z}$ direction the magnetic field point towards the center of the trap; in the $\hat{x}$ and $\hat{y}$ direction they point away from the center of the trap. In order to compensate for this flip in the gradient of the Zeeman potential we flip the polarity of the light. σ^+ light comes from the $\hat{x}$,$\hat{y}$ and $-\hat{z}$ directions. σ^- light comes from the $-\hat{x}$,$-\hat{y}$ and $\hat{z}$ directions.

Further when we have already created a trap, the restoring force of atoms in the MOT is linear. We can therefore view the system as a harmonic oscillator and solve for a basic relation:[11]

$$3/2k_bT = 1/2mv_{rms}^2 = \kappa z_{rms}^2 \tag{4.7}$$

With κ a MOT-dependent constant that goes linearly with magnetic field. This indicates that when we turn up the magnetic field, either the MOT must compress at the square root of the rate of magnetic

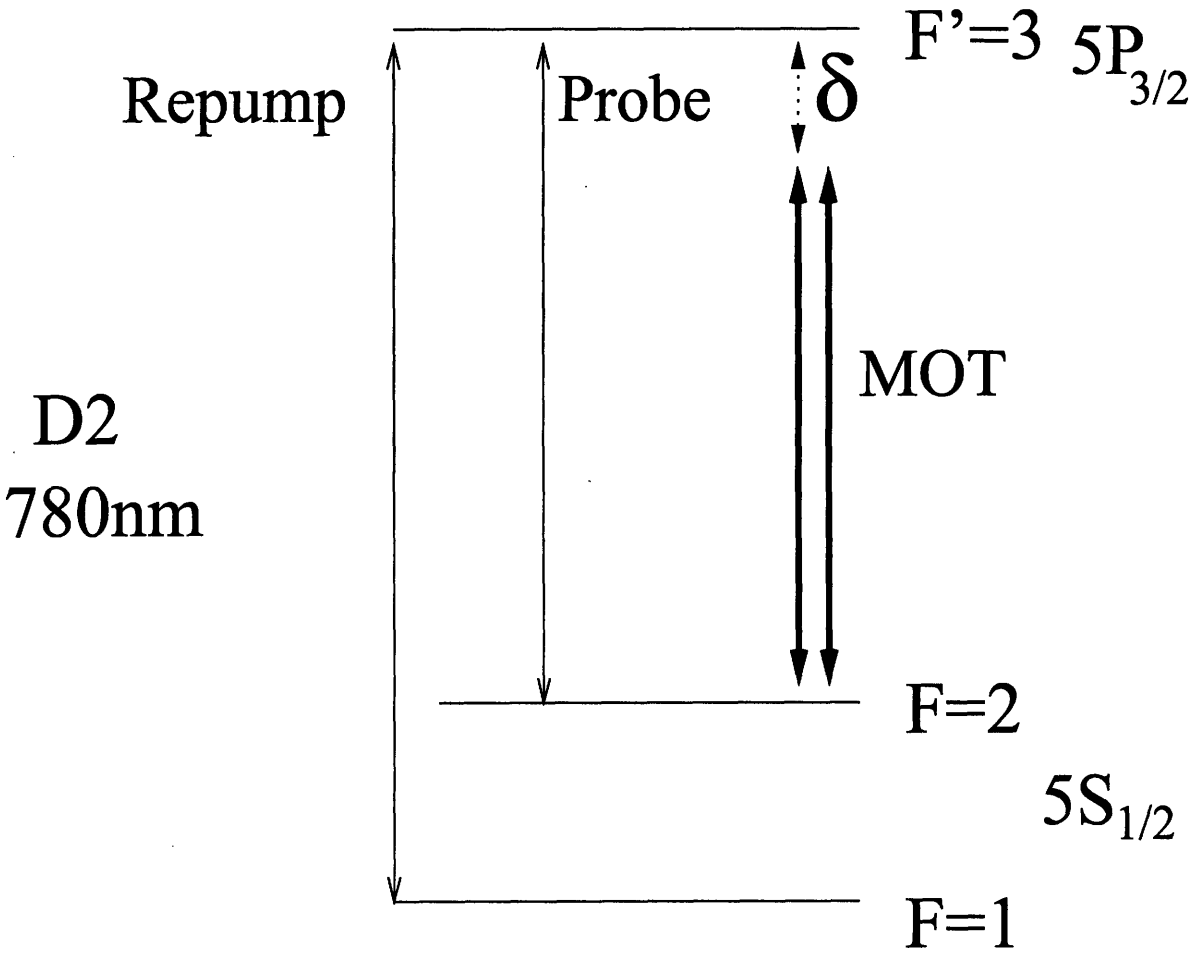

Figure 4-3: Transitions Probed in the MOT

field increase, or the temperature must diminish. Either situation is desirable.

4.2 The Practical MOT

To practically achieve a MOT two different lasers tuned to two different frequencies are used. These two lasers as seen in figure 4-3 are the pump (or MOT) and the repump laser. There is a third laser, the probe laser, which is used for spectroscopy. We use the (F=2 to F'=3) transition in ^{87}Rb to make our MOT. We use this transitions because

it is a closed transition. Light in the $5^2P_{3/2}$ $F' = 3$ state cannot decay into the $F = 1$ ground state. The cycling transition can be broken by spontaneous decay from the $F = 2$ ground state to the $F = 1$ ground state. We therefore couple the $F = 1 >> F' = 3$ transitions with the repump laser. The probe laser is a weak laser that is on resonance to the $F = 2 >> F' = 3$ transition which we use to probe the absorption spectrum of the MOT cloud.

We use the TEC 300 tapered laser diode produced by Sacher Lasertechnik Group for our pump laser. The advantage of a tapered laser diode is that it can produce up to 800 mW of power. This laser has as its default wavelength 780 nm. At the MOT it's power is 80 mW. We split this equally along each of the three axes, ad retro-reflected it with a mirror. The retroreflection flips the polarization of the light. The trap sees about 53 mW in perpendicular direction, for a total of 160 mW of trapping power.

We use a TEC 50 DFB laser produced by Sacher Lasertechnik for our repump laser. This laser has as its default wavelength 780.2 nm. At the MOT we again split it along the three axes and retro-reflect it. The MOT therefore sees 12 mW of power from the repump laser, about 4 mW in each direction.

We use an Extended Cavity Diode Laser at very low power for our probe laser. We run it at a few orders of magnitudes under the saturation intensity of ^{87}Rb in order to not saturate our photodetector.

4.2.1 Magnetic Fields

In our MOT we have two sources of Magnetic fields. These are the anti-Helmholtz coils, the theory of which I outlined above, and bias-field magnetic coils. I will briefly discuss how we use these. A more detailed approach can be found in [3].

The formula given above in eq:4.5 is not exactly accurate. The actual magnetic fields of an anti-Helmholtz coil is given by:

$$B_\rho = \mu_0 I \left[-\frac{3}{2}\frac{DR^2}{(D^2+R^2)^{5/2}}\rho + \frac{15}{16}\frac{R^2(4D^2-3R^2)}{(D^2+R^2)^{9/2}}(\rho^2 - 4sz^2) \right] \quad (4.8)$$

$$B_z = \mu_0 I \left[3\frac{DR^2}{(D^2+R^2)^{5/2}}z + \frac{15}{24}\frac{R^2(4D^2-3R^2)}{(D^2+R^2)^{9/2}}(4z^3 - 6\rho^2 z) \right] \quad (4.9)$$

The coil we use has 30 turns. Each coil has radius R=2.2 cm and separation 2D=4.3 cm. We can therefore find the magnetic field and magnetic field gradient at a given current. Figure 4-4 shows these for a current of 5 Amperes. Note that the magnetic field scales with current so these figures are extensible to other currents. The magnetic field gradient is twice as strong in the z direction; this is as our simple analysis in equation 4.5 suggests.

It's worth noting that though I refer to the main axis of the MOT coils as the z-direction, this is just by convention. The actual strong axis of the quadrupole trap is parallel to the ground and thus might be more accurately referred to as the x-direction.

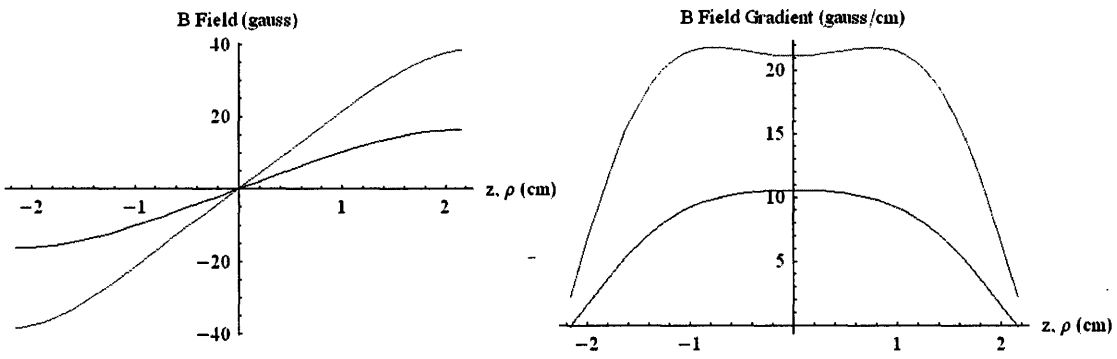

Figure 4-4: The Magnetic Field and its Gradient for the MOT Coils
B_z is in red. B_ρ is in blue.

Figure 4-2 suggests that wherever the magnetic field is zero should correspond to the center of the trapped cloud of atoms. Therefore if we moved the zero of the magnetic trap adiabatically we can also move the clouds of atoms. We also need to compensate for the earth's magnetic field of approximately one gauss. We do this by three sets of Helmholtz coils; each set is arranged along a different axis of the trap.

As later parts of experiment are oriented vertically and must also compensate for the Earth's magnetic field, our z bias coils are larger and thus more powerful. They have side-lengths of 11 inches and are separated by 3.5 inches. The x and y coils have side-lengths of 4 inches and separations of 8.5 inches. Figure 4-5 shows the magnetic field and magnetic field gradients for the bias coils. The magnetic field gradient is less than 1% of the gradient of the MOT coils.

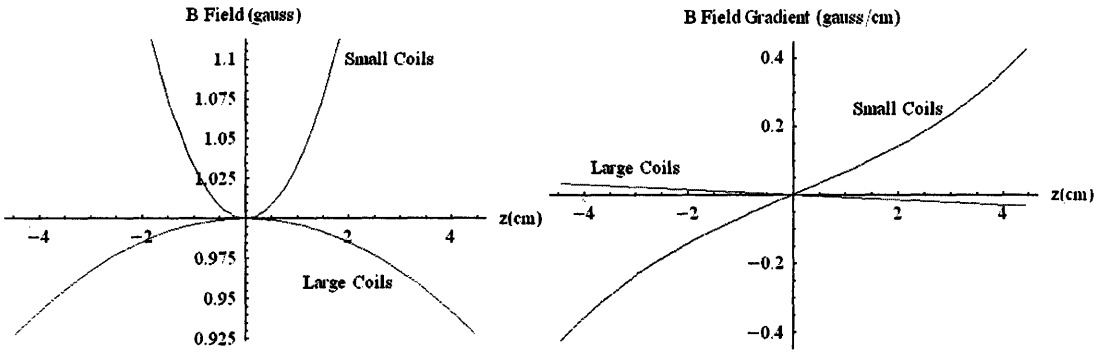

Figure 4-5: Magnetic Field and its gradient for Bias Coils
Here the current for the bias coils is calibrated so that the B-field at z=0 is one gauss.

4.3 Time of Flight and Atom Count in the Trap

After we make a MOT and polarization gradient cool the atoms, it is of interest of us to determine the temperature and the number of atoms in the cloud. This information can be determined from looking at imagery taken of the MOT with a CCD camera, and analyzing the pixel by pixel optical depth. See figure 4-6 for such an image. Optical depth, OD, is defined as:

$$I/I_0 = e^{-OD} \tag{4.10}$$

where I is the observed intensity and I_0 is the source intensity. Optical depth can be further related to number of atoms by:

$$OD = \sigma \int n \cdot dl \tag{4.11}$$

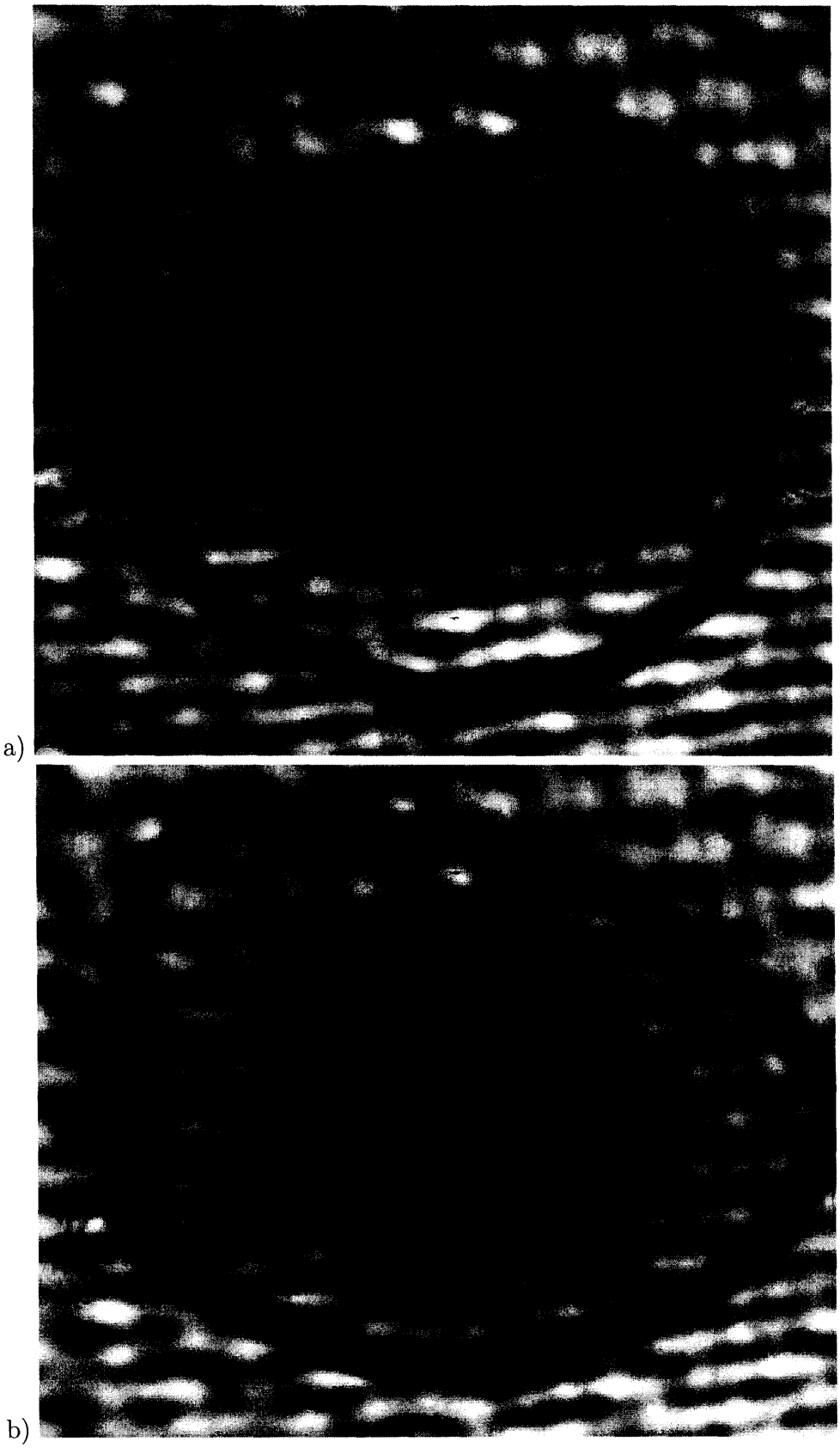

Figure 4-6: MOT Clouds
a) is the trapped MOT cloud. b) Is the MOT cloud 3 ms after we release trapping field. Comparing the size of the cloud in a) and b) gives us the velocity of the cloud and therefore its temperature. Examining the optical depth of the cloud in a) gives

n is the number of atoms per unit volume. l is the distance parameter (i.e. the depth of the cloud. σ is the absorption cross-section.

$$\sigma = 6\pi(\lambda/2\pi)^2 \tag{4.12}$$

Here, λ is the transition wavelength. This particular formulation assumes that the saturation parameter, $s_0 << 1$, and that the detuning, $\delta = 0$. These are not bad assumptions for a probe laser. This equation can be found in many elementary atomic physics textbooks (i.e. [4]). We then assume that, $n(l)$, our distribution of atoms in the cloud is roughly Gaussian. We can measure the size of the cloud using our camera. In particular, our cloud after compression is .5mm wide along the strong axis and 1mm wide along the weak axes.

Using this information we found that after MOT cooling there were $\approx 10^7$ atoms trapped. After polarization gradient cooling there were $\approx 3 \times 10^6$ atoms trapped. These figures are in line with what we expect in a MOT[14].

We can also perform time-of-flight spectroscopy using images from the camera. We take images at multiple points in time and examine how the gas expands after turning off the trap. A treatment of this can be found in Yavin et al.[18]. One assumes that the gas obeys a Maxwell-Boltzmann distribution and that it is falling due to gravity. Then one back-solves for the average velocity in the orthogonal directions your camera can see. Doing this we found:

$v_v = 8.4$ cm/s. The vertical velocity.

$v_h = 8.0$ cm/s. The horizontal velocity.

The reasons these two numbers are different is that the trapped cloud of Rubidium is not itself isotropic; it is trapped more tightly in the horizontal direction.

From these figures we can calculate the temperature of the cloud using:

$$1/2k_bT = 1/2mv^2 \tag{4.13}$$

Given that the mass of ^{87}Rb is 1.443×10^{-25} kg[15] we find that:

$T_v = 73.8\ \mu$K

$T_h = 66.8\ \mu$K

Which is sufficiently cold to trap in an optical dipole trap.

4.4 Optical Pumping

Recalling the procedure outlined in chapter 2, after we have our cold cloud of atoms we must magnetize it. We do so using optical pumping. We tune a D1 laser to the F=2 to F'=2 transition in ^{87}Rb. The laser is σ^+ polarized; every time a laser photon interacts with an atom, $\Delta m_f = 1$. As emission has no preference for changes in m_f, we should expect that over long periods of time the atoms should reach the $m_f = 2$ ground state. See figure 4-7. This ground state is a "dark state" that cannot absorb the D1 light. The $F = 1$ ground state is another "dark state" for this D1 light. It is therefore necessary to pump the atoms

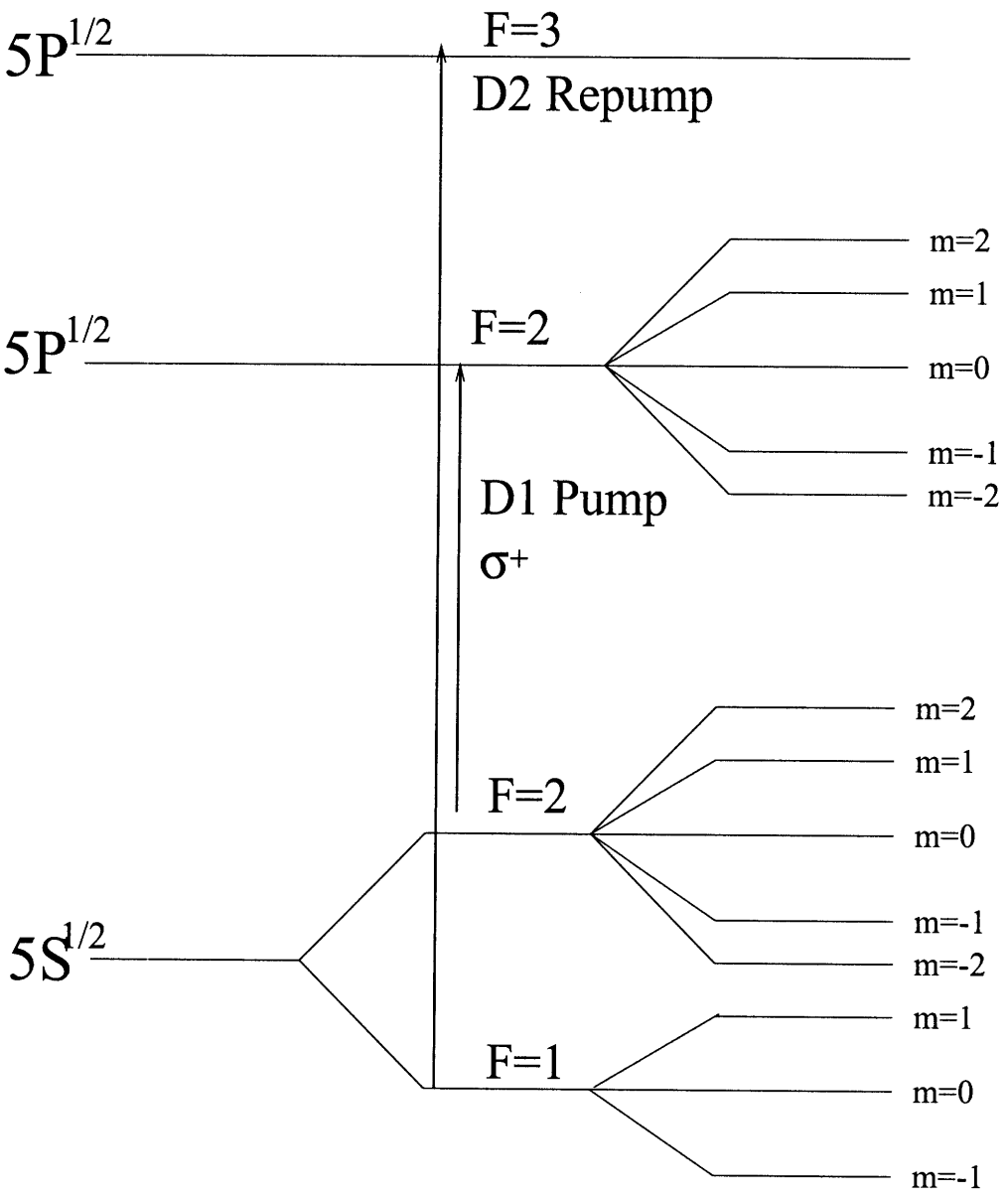

Figure 4-7: Optical Pumping on the D1 Line
We optically pump our Rubidium on the D1 line into the m=2 ground state. We use the repump laser to expel atoms that fall into the F=1 state.

out of this state. We do so using our $F = 1 >> F' = 3$ repump laser. Recall that the $(F' = 3 >> F = 1)$ state is forbidden. Therefore this repump laser will restore the atoms that fall into the $F = 1$ state to the $F - 2$ state.

We have created an ultra-cold (≈ 40 μK) compact (.5mm $\times$ 1mm) cloud of ^{87}Rb vapor which we have magnetized into the $m = 2$ state. All that remains is to load it into the optical fiber.

Chapter 5

Optical Dipole Trap

5.1 Optical Dipole Traps

The other trapping mechanism we use in our experiment is a red-detuned optical dipole trap. When far-detuned the effect of the laser can be treated as solely that of second order perturbation theory; that is to say, small.

Consider a two state atom. According to perturbation theory, the states of that system acted on by perturbation H_1 should be shifted in energy by:

$$\sum_{j \neq i} \frac{|\langle j|H_1|i\rangle|^2}{E_i - E_j} \tag{5.1}$$

Consider $H_1 = -\hat{\mu}\vec{E}$ to be the electric dipole operator. In the dressed atom approach in which we consider the atom and the field to be a combined system, $E_i = n\hbar\omega$, where n is the number of photons and ω is the laser frequency. Note that the dressed atom approach requires that n be very large. In the excited state a photon is absorbed so

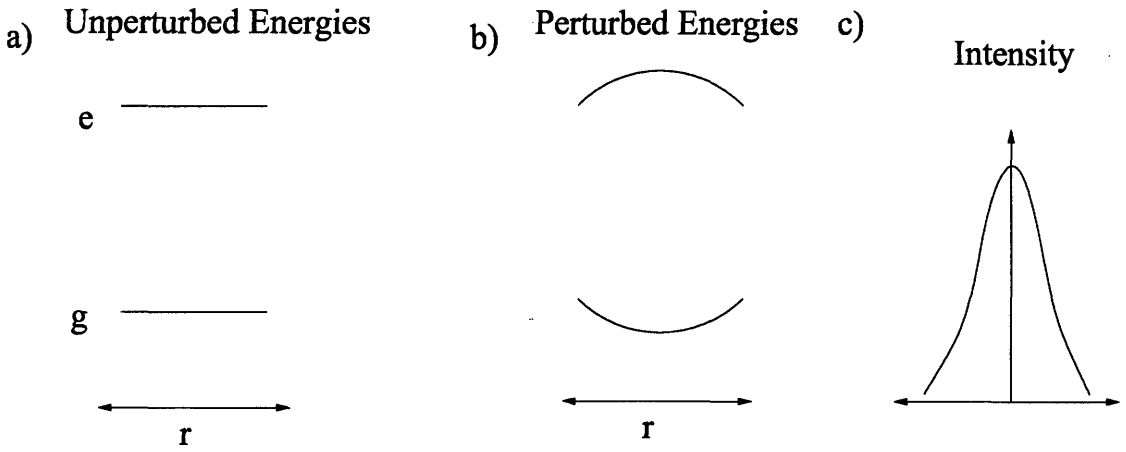

Figure 5-1: Light shifts for a Two Level Atom
a) Shows the energies of the unperturbed state. b) shows the energies of the light-shifted states as they vary with position. c) shows the corresponding intensity profile of the laser. b) and c) should be taken as schematic representations.We can see that the ground state will act as a trap for atoms, while the excited state will expel such atoms.

that the field energy is diminished by $\hbar\omega$, and $E_j = \hbar\omega_0 + (n-1)\hbar\omega$. Therefore $E_i - E_j = -\hbar\delta_{ij}$.

Performing the perturbative calculation then gives us:[9]

$$\Delta E = \pm\frac{3\pi c^2}{2\omega_0^3}\gamma\delta I \tag{5.2}$$

Where γ^{-1} is the natural lifetime of the excited state, which can be related directly to the dipole matrix element. Consider that the intensity is not uniform but decays in a Gaussian pattern about some central point; for red-detuned light we should then find that there is now a potential well in the ground state as shown in figure 5-1b.

The result in eq:5.2 only holds for a two state system. Consider that our actual dipole trap laser is set to 784 nm, which puts it between the D1 and D2 transitions of Rubidium. This indicates that the ground

state should be trapping for the D2 transition and repelling for the D1 transition. Ultimately we must be careful that the sum of these two dipole shifts still results in trapping in the ground state.

5.1.1 Trapping Potential

Following the math in [9], we can actually derive the trapping potential for an alkali atom such as rubidium. In particular the light shift can be written as:

$$\Delta E_i = \frac{3\pi c^2 \Gamma}{2\omega_0^3} I \times \sum_j \frac{c_{ij}^2}{\delta_{ij}} \tag{5.3}$$

Where c_{ij} are the line strengths. If $P = 0, \pm 1$ is the polarization of the dipole trapping laser, and m_f is the spin number of the ground state then:

$$U(r) = \frac{\pi c^2 \Gamma}{2\omega_0^3} \left(\frac{2 + P m_f}{\delta_{D2}} + \frac{1 - P m_f}{\delta_{D1}} \right) I(r) = A I(r) \tag{5.4}$$

δ_{D2} and δ_{D1} are the detuning of the $5P^{3/2}$ and $5P^{1/2}$ relative to the the dipole light frequency ω, respectively. This derivation is only correct if the detuning, δ, is much larger than the hyperfine splitting of the excited states.

Similarly, we can find the scattering rate for the alkali atom to be:[9]

$$\Gamma_{sc} = \frac{\pi c^2 \Gamma^2}{2\hbar\omega_0^3} \left(\frac{2}{(\delta_{D2})^2} + \frac{1}{(\delta_{D1})^2} \right) I(r) \tag{5.5}$$

We use linear polarized light due to the m_f dependent splittings that using circularly polarized light would introduce. It is possible to

increase trap depth using polarized light as equation 5.4 implies. This would have complications in that we would need to be more certain of the magnetization of the Rubidium; likely we would have to continue to optically pump far later in the experiment.

5.1.2 Oscillation Frequency

We can then attempt to make a calculation of the oscillation frequency of our trap. Let us take our light intensity to be of a Gaussian profile:

$$I(r) = I_0 e^{\frac{-r^2}{d^2}} \tag{5.6}$$

The data sheet for our fiber tell us that at $r = 2.5\mu$, $I = e^{-1} I_0$. Therefore $d = 2.5\mu$. An image of the actual intensity profile of the fiber can be seen in figure 5-2.

Our potential has a restoring force:

$$F(r) = -\nabla U(r) = 2A\frac{I_0}{d^2} r e^{\frac{-r^2}{d^2}} \tag{5.7}$$

For atoms that are very tightly trapped, $r \ll d$, the restoring force is linearly dependent on r. We can then model the atoms as resonating in a harmonic trap with frequency ω_{trap}. As:

$$F(r) = ma = m\omega_{trap}^2 r = 2A\frac{I_0}{d^2} r \tag{5.8}$$

$$\omega_{trap} = \sqrt{(A\frac{I_0}{md^2})} \tag{5.9}$$

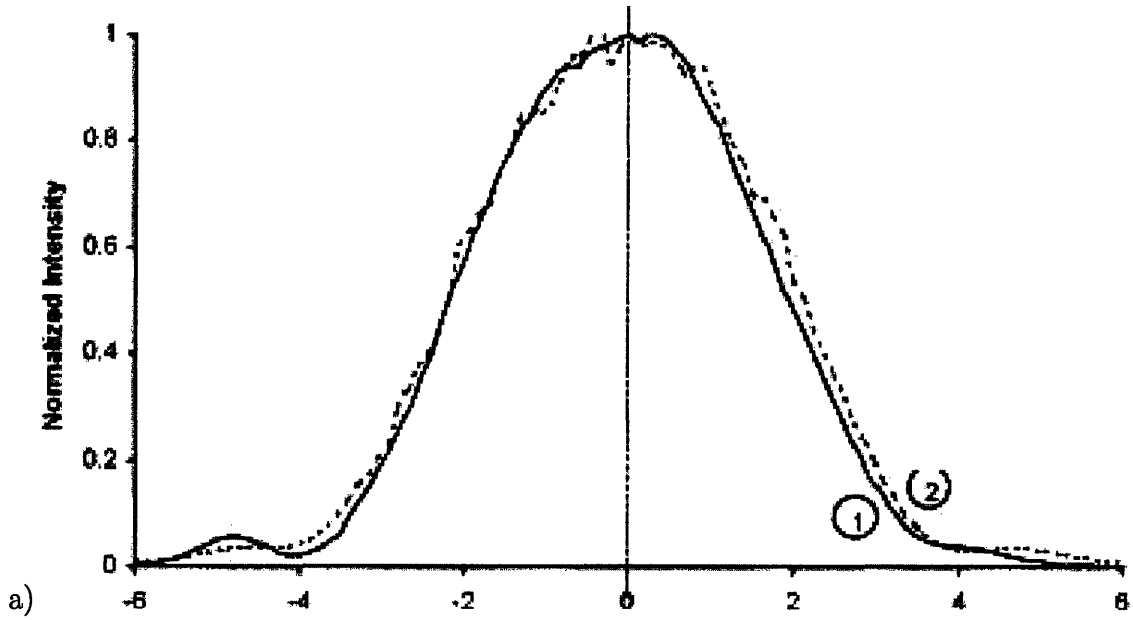

a)

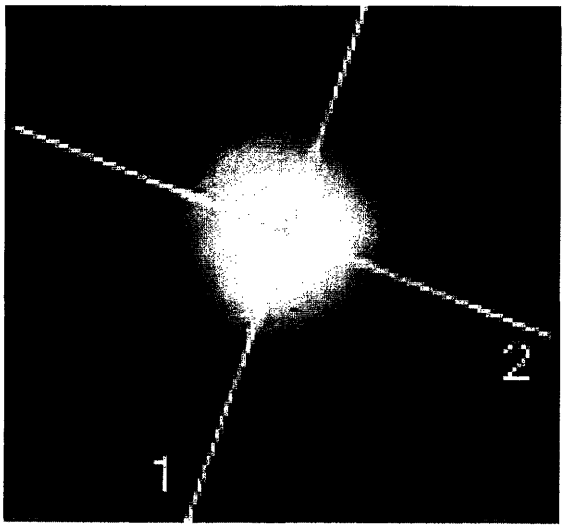

b)

Figure 5-2: Intensity Profile in Fiber
Note that the core diameter is only 6.8 microns. The intensity profile is roughly Gaussian.

Even if our atoms are not so tightly trapped, $\tau = \omega_{trap}^{-1}$ is still a good time scale for the motion of the atoms in the trap.

We now calculate I_0. As:

$$P = \int I \cdot dA = I_0 \int dr d\phi r e^{\frac{-r^2}{d^2}} = \pi I_0 d^2 \tag{5.10}$$

$$I_0 = \frac{1}{\pi d^2} P \tag{5.11}$$

Where P is the power of the beam. We now have enough information to calculate the parameters discussed above.

5.1.3 Calculation of Trap Parameters

Let us take the power of the diode trap at the laser to be $6.5 \pm .5$mw at the fiber. Let us take $d = 2.5\mu$. Then we find:

$I_0 = 3.57 \pm .32 \times 10^5$ mW per m^2.

Assuming that there our diode laser is at 785 nm and using $\Gamma = 38.11$ MHz and $\omega_0 = 2\pi \cdot 384.231$ THz (corresponding to the D2 transition), we find that:

$A = 3.97 \times 10^{-33}$ m^2 sec.

With similar values for the D1 line:

$A = 3.96 \times 10^{-33}$ m^2 sec

Which are almost identical. We then find a trap depth of:

$T = 1.02 \pm .10$ mK

Our scattering rate is:

501 ± 45 Photons per second.

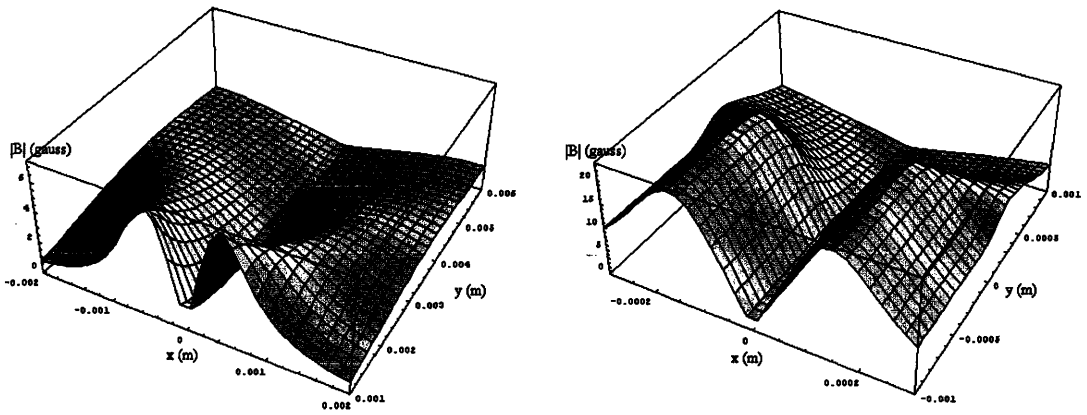

Figure 5-3: Magnetic Field of Funnel Trap
The y-axis corresponds to the direction that is aligned with the fiber. The first image is of the magnetic field from 1 mm to 6 mm above the chuck. The second image shows the magnetic field from 1 mm above the chuck to 1 mm inside the fiber.

And our resonant frequency is:

$\omega_{trap} = 177 \pm 8$ KHz

5.2 Trap Mechanics

Once we have the atom cloud cooled and trapped, it is time to load it into the fiber. We move it using a quadrupole magnetic field produced by four taut wires of thickness 280μ emanating from a single point. These wires fan outward at angle of 33° to a hight of 3.9 cm from the top of the chuck that holds the fiber. Both the chuck and wire can be clearly seen in figure 2-1. The magnetic field that this trap produces, as derived from the Biot-Savart law, is shown in figure 5-3 for a current of 1 A through the funnel wires.

When we turned off the magnetic field of the MOT and turned on the magnetic field of the funnel, an interesting effect occurred; the atom

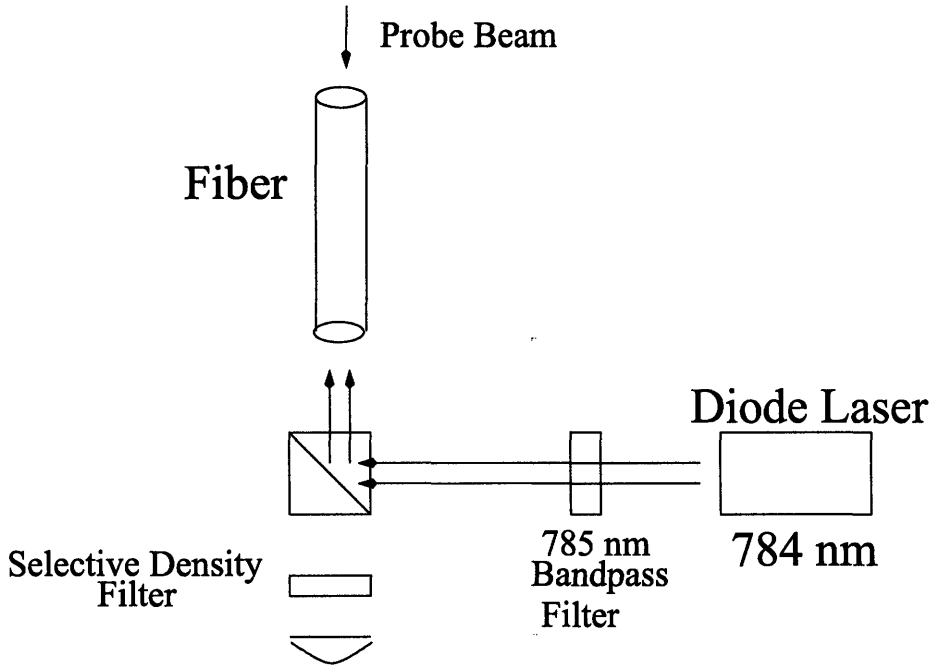

Figure 5-4: Optical Schematic for Fiber

cloud began to fall with gravity into the funnel, but then bounced up again. This is a result of angular momentum conservation. As it falls the action of the funnel makes it more and more compact, causing it to spin faster. The resulting change in the angular momentum gives it a restoring force to oppose gravity. Further explanations of this phenomenon can be found in [10].

To correct for this phenomenon we kept the MOT coils on during the loading process so that the atom cloud did not become less compact and thus vulnerable to this process. This has the unfortunate effect of hastening diffusion heating of the cloud.

5.2.1 Fiber Optics

Figure 5-4 is a schematic representation of the optics entering the fiber. The diode laser produces light at near 784 nm. We filter this light with a 785 nm bandpass filter produced by SEMROCK. It enters the fiber. We send a probe beam from the opposite direction. This beam is either on the D1 or D2 line, depending on which transition we wish to probe. Its intensity is kept to less than 4 million photons per second as that is the saturation limit of the photodetector. Upon exiting the fiber it goes through a selective filter. The reason we use this filter is that the dipole laser reflects off of the top of the fiber. As its intensity is large we need to filter out photons at the laser diodes frequency, lest it saturate the detector. We do so using frequency selective filters. For the D1 line we use a 790 nm long pass filter. For the D2 line we use a 780 nm bandpass filter. Both are made by SEMROCK.

5.3 Phase Space Density

The phase space density is a measure of the quality of our atom trap. Phase space density can be described as:

$$PSD = n \cdot \lambda_{DB}^3 \tag{5.12}$$

Where λ_{DB} is the De Broglie wavelength and n is the density of atoms. The density of atoms can be derived from equation 4.11 based on the optical depth of the atoms. The De Broglie wavelength is derived from

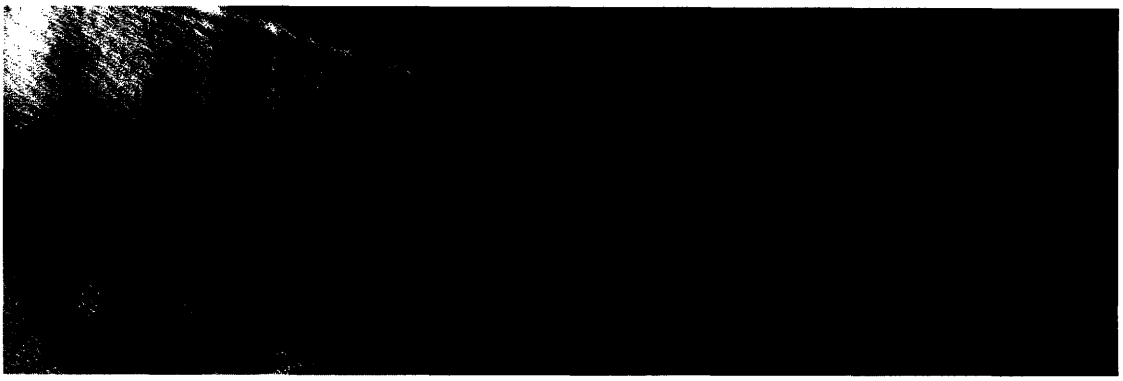

Figure 5-5: Atoms in the Funnel Trap
This is an image of the absorption spectrum of our funnel trap. The dark spots in the center of the funnel correspond to the atoms in the MOT cloud.

the temperature. This can in turn be derived using the potential energy of the magnetic trap and the virial theorem relationship that if:

$$V(r) = \alpha r^n \tag{5.13}$$

Where α is some constant, than:

$$2\langle T\rangle = n\langle U\rangle \tag{5.14}$$

5.3.1 Calculation of Phase Space Density and Temperature

We take the image given in figure 5-4 and divide the point by point optical density by the optical density of a background image. To give us the optical density, OD, which depends on position, we take slices of the distribution with thickness, δy and find the mean $OD(z)$ within each slice. We then fit $OD(z)$ to a Gaussian:

$$OD(z) = ae^{-\frac{(z-z_0)^2}{w^2}} \tag{5.15}$$

We can then integrate the total number of atoms in a slice:

$$N = \sqrt{\pi} a w \frac{\Delta y}{\sigma} \tag{5.16}$$

We now have the number of atoms in a slice,N, the fitted width of the slice, w and the length of the slice, Δy. This allows us to get the density in a given slice, n. Using the Virial theorem and that the average energy is $k_b T$ we can find the temperature:

$$T = \frac{\mu_B \omega}{2k_b} \frac{dB}{dz} \tag{5.17}$$

And the phase space density:

$$PSD = D \left(\frac{2\pi\hbar^2}{m k_b T} \right)^{3/2} \tag{5.18}$$

Using this analysis we found that temperature was near 1 mK at the fiber and the phase space density was $\approx 10^{-7}$ at the fiber. A more detailed account of this can be found in[3].

5.4 Optical Depth of the Dipole Trap

If you recall the discussion in the first chapter of this thesis, the reason we wish to trap atoms in the fiber is to enhance their optical depth. Reiterating the equation for optical depth:

$$OD = \sigma \int n \cdot dl \tag{5.19}$$

Where σ is the cross-section of the atom, n is the number of atoms per unit volume and l is the length element.

If $n(l)$ is uniform than:

$$\int n \cdot dl = nl = \frac{N}{A \cdot l} l = \frac{N}{A} \tag{5.20}$$

Where A is the area the atoms are confined to and N is the number of atoms. The optical depth is now:

$$OD = \sigma \frac{N}{A} \tag{5.21}$$

Because OD is inversely proportional to area of confinement, by confining the atoms to a fiber six microns in diameter, we vastly increase the optical depth. What we can actually measure, via absorption of the probe beam, is the optical depth.

Chapter 6

Results and Conclusions

Over the last several chapters, the formalism of our experiment has developed. Several preliminary results about the nature of our trapping scheme have been presented as well as theoretical results for our trap behavior. The question then becomes: have we trapped the atoms in our optical dipole trap?

6.1 Results

We do have reason to believe we have trapped the Rb inside of the fiber. A graph of this information can be seen in figure 6-1. Note that the peak of absorption is detuned from where we expect free atoms to have their absorption peak. This detuning is the result of the AC Stark shift as detailed in eq.5.4. Note also that the trapped atoms can be found at multiple detunings. This is also expected as our atoms are warm($\approx$ 1mK) compared to the trap depth of 1mK. We therefore expect the atoms in the fiber to be not particularly well confined to

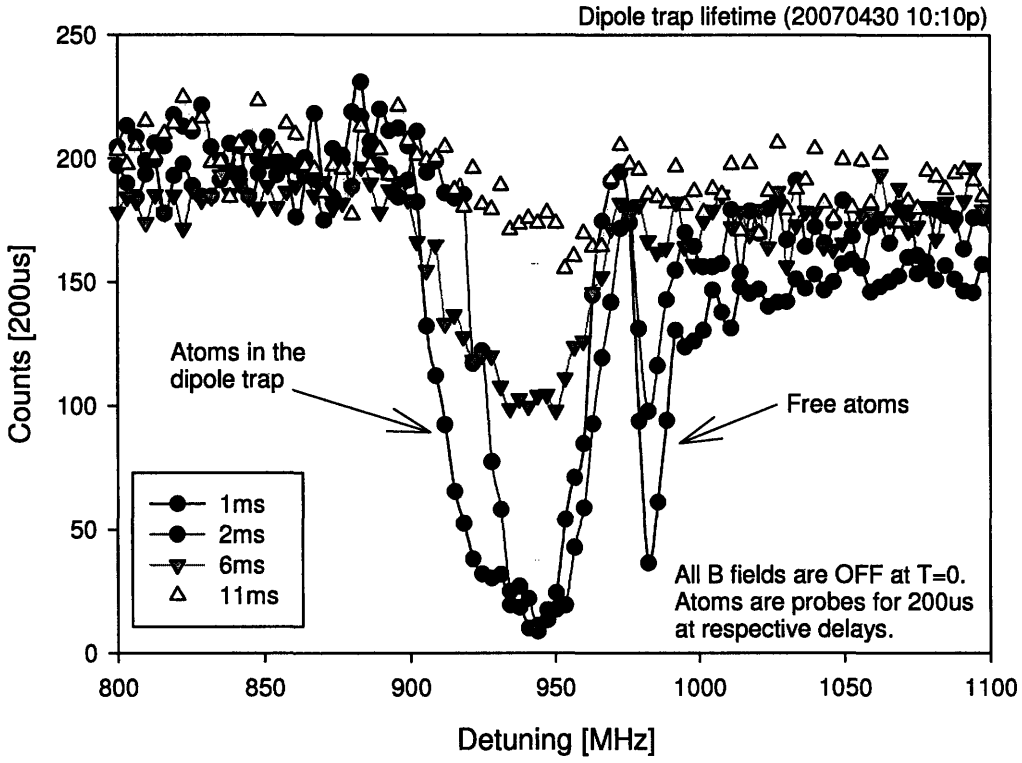

Figure 6-1: Preliminary Data on Trap Lifetime

The x-axis is the frequency detuning of the probe laser from some arbitrary frequency. The y-axis is the counts on our photo-detector and is therefore related to optical depth. This data is taken at 1 ms, 2 ms, 6 ms and 11 ms after we have trapped the atoms. We used the $F = 2$ to $F' = 3$ D2 line of Rubidium to probe the atoms. Note that there is still a significant absorption dip 6 ms after the atoms become trapped.

the center of the dipole traps. Those that are further from the center would have different detunings and this results in the broadening seen in figure 6-1.

But it is possible for the atoms to be trapped in the dipole trap but not in the fiber. The region directly outside the fiber also may act as a dipole trap. However if we are trapped in that region we expect a small lifetime as there is no confinement in the z-direction. Gravity should unload the trap. If the atoms are trapped outside the fiber it should unload it in less than 1 ms. If they are inside the trap, the trap lifetime is determined by the length of the trap. The fiber is 1.3 inches long. If we take an atom at rest at top of the fiber and let it fall due to gravity, we should find that it would take ≈ 6.7 ms to exit the trap. This time scale is consistent with the data seen in figure 6-1.

6.1.1 Number of Atoms

So far we have been unable to determine the number of atoms in the trap. Once optical depth is large enough it is virtually impossible to determine it based on resonance: to a photodetector OD=10 and OD=20 are both below background levels. Only 30 atoms would be needed to provide an optical depth of one. We currently believe that we have somewhere between 100 and 5000 atoms trapped in the fiber. We therefore would like to look off-resonance, where we should expect absorption as well. Unfortunately we have currently not been able to separate out the effects of broadening due to variable AC Stark shifts and broadening

due to large optical depths. There is the further problem of separating out absorption of atoms in the trap from absorption due to atoms remaining in the magnetic funnel trap.

There is also some problem in our data in that we believe that our atoms may be altering the polarization of light in the probe beam. As we send our probe beam through a polarizing beam-splitter this is skewing our results. Preliminary work done that compensates for this effect is proving fruitful.

6.2 Future Work

The basic problem we are facing is that the high temperature of the atoms is resulting in difficult-to-resolve peaks in the absorption spectrum. In the short term we are attempting to deal with this problem by modulating the laser at a frequency much larger than $\omega_{trap} = 177 \pm 8$ KHz. This frequency represents the rate at which the atoms slosh back and forth in the trap. A laser modulation at a frequency ten times this will not impact their motion, though it will diminish the effective depth of the trap by half as compared to using the laser in CW mode. We will then only detect photons in the period of time when the laser is modulated off. This will greatly diminish the Stark broadening effect on the absorption spectrum.

Longer term we are considering changing to a laser of longer wavelength to diminish the scattering rate, currently 501 ± 45 photons per second. Every scattering event from the diode laser leads to heating of

the trapped sample and expels some of our atoms out of the F=2 state that we are probing. Equation 5.4 tells us that while greater detuning diminishes trap depth with δ, equation 5.5 tells us that scattering rate diminishes with δ^2. If we move to a laser of 805 nm, our trap depth decreases by 47% but our scattering rate is reduced by 90%. We simply need our 805 nm laser to be twice as powerful as our current 785 nm laser and the trap will be improved.

Finally we may wish to implement some scheme that cools the atoms in the funnel trap. Most of our heating is provided by moving the atoms down the magnetic gradient in the funnel trap. We would have a far cleaner signal if the atoms were still at $\approx 70\ \mu K$ in the trap.

Appendix A

Rubidium Spectroscopy

Table A.1: D1 and D2 line for Rubidium.

This table gives the isotope shift for these transitions for ^{85}Rb and ^{87}Rb. This data comes from [1]

	^{85}Rb (MHz)	^{87}Rb (MHz)	Isotope Shift (MHz)
D1 line	377 107 385.623(50) MHz	377 107 463.209(50)	77.586(70)
D2 line	384 230 406.528(50) MHz	384 230 484.468(10)	77.940(50)

Table A.2: Relative D1 Transitions

All figures derived from the information in figure A-1 and table A.1.

Transition	ΔFrequency (MHz)	Isotope	Notes
(F=3 to (F'=2,F'=3))	0	^{85}Rb	Reference Laser. Crossover peak.
(F=1 to F'=2)	5949.1	^{87}Rb	
(F=2 to F'=1)	5136.6	^{87}Rb	
(F=2 to F'=2)	885.6	^{87}Rb	Optical Pumping Transition
(F=2 to F'=1)	108.1	^{87}Rb	

Table A.3: Relative D2 Transitions

All figures derived from the information figure A-1 and table A.1.

Transition	ΔFrequency (MHz)	Isotope	Notes
(F=3 to (F'=3,F'=4))	0	^{85}Rb	Reference Laser. Crossover peak.
(F=1 to F'=3)	5501.8	^{87}Rb	Repump Laser
(F=2 to F'=3)	5136.6	^{87}Rb	MOT Transition

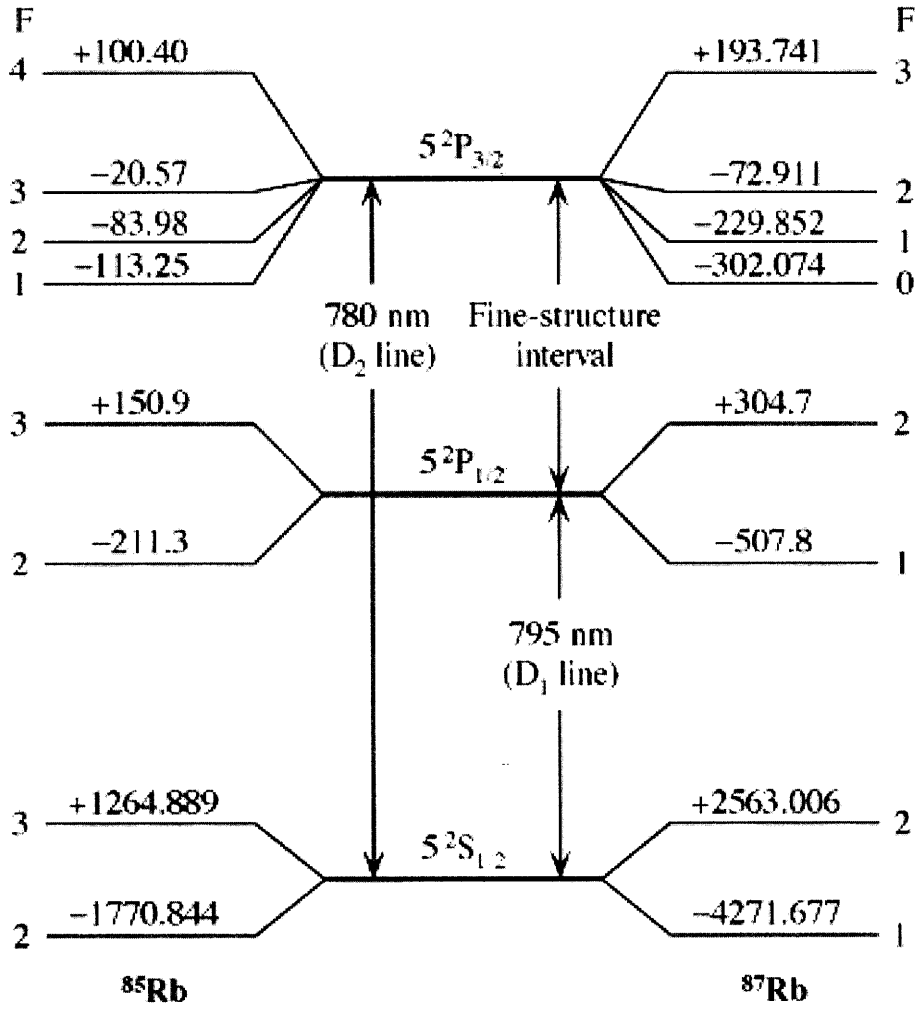

Figure A-1: Level Diagram for Rubidium

Data comes from [1].

Appendix B

PI Controller Board

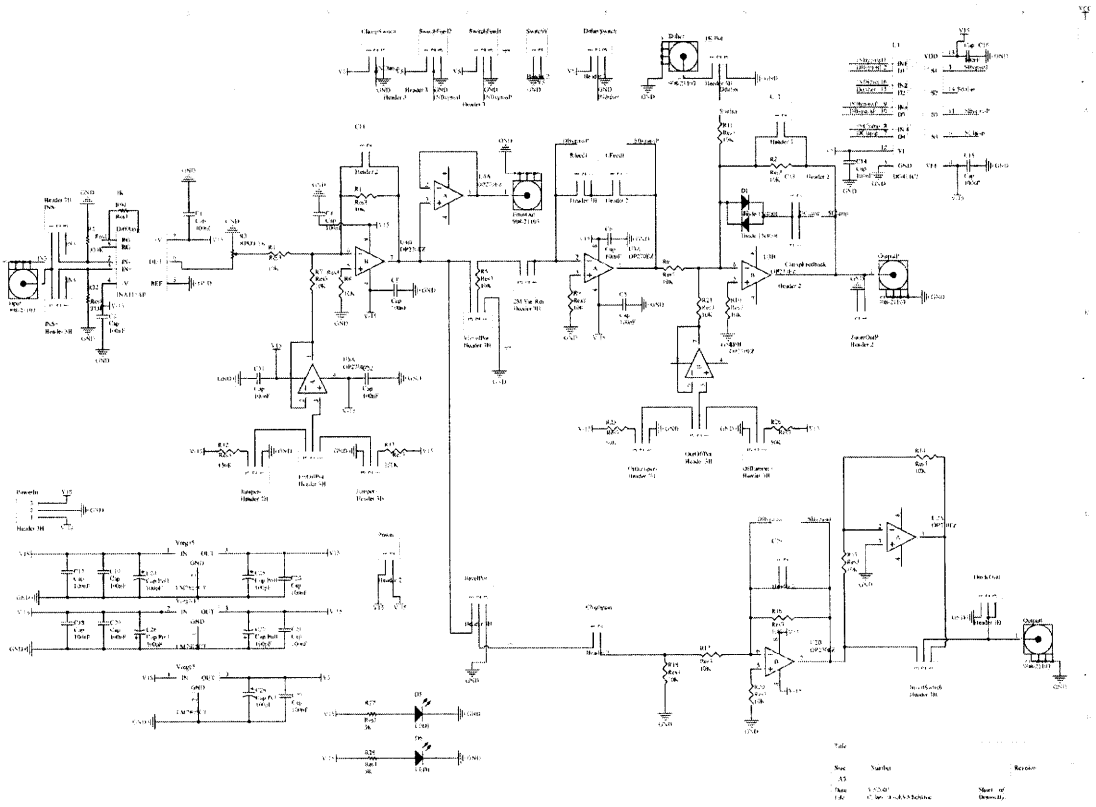

Figure B-1: PI Controller Board Schematic

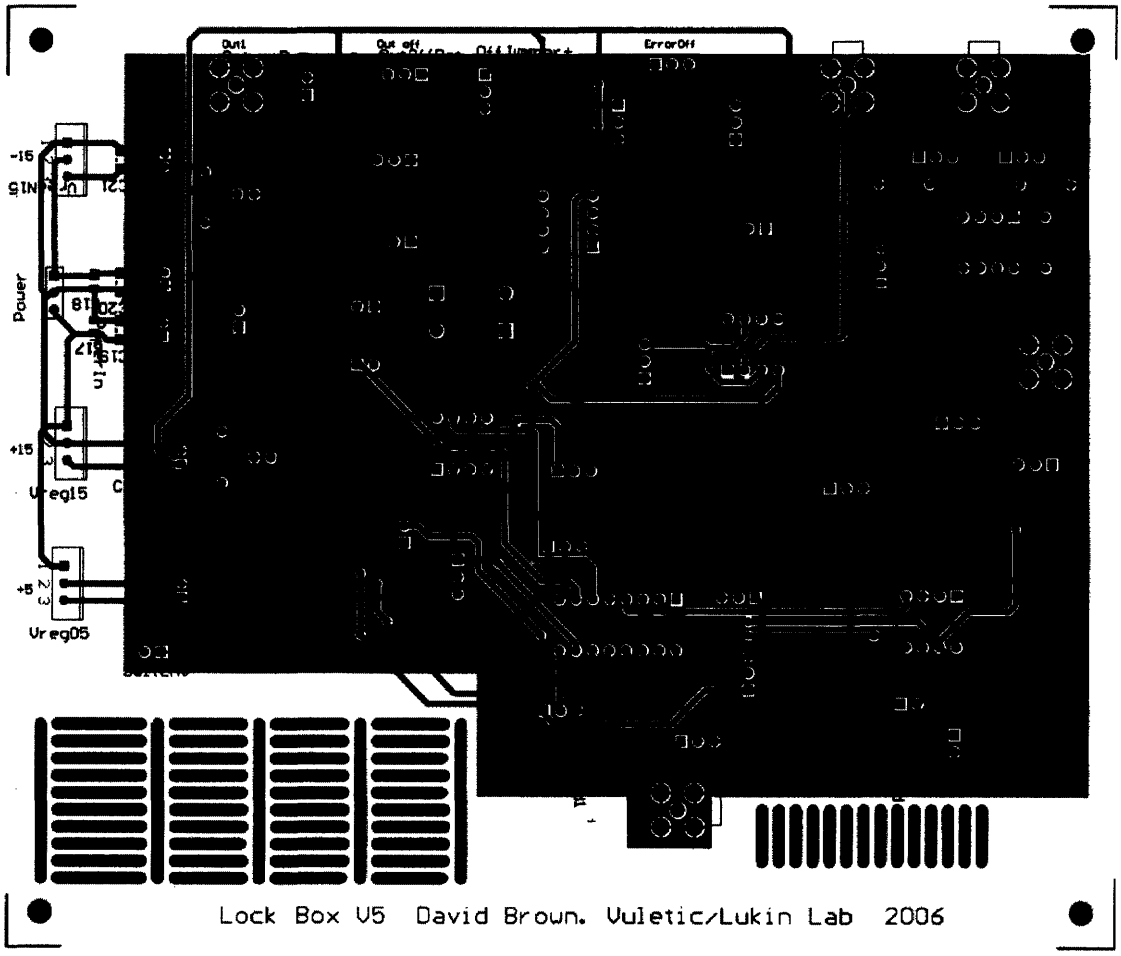

Figure B-2: PI Controller Board PCB

Bibliography

[1] Ayan Banerjee, Dipankar Das, and Vasant Natarajan. Precise fine-structure and hyperfine-structure measurements in rb. arXiv:physics/0209019, 2002.

[2] Danielle A. Braje, Vlatko Balic, G. Y. Yin, and S. E. Harris. Low-light-level nonlinear optics with slow light. *Physical Review A*, 68(041801), 2003.

[3] Yiwen Chu. Loading rubidium atoms into a hollow core fiber. Undergraduate thesis, MIT, 2007.

[4] Claude Cohen-Tannoudji, Jacques Dupont-Roc, and Gilbert Grynberg. *Atom-Photon Interactions.* Cambridge University Press, 2006.

[5] Kristan L. Corwin, Zheng-Tian Lu, Carter F. Hands, Ryan J. Epstein, and Carl E. Weiman. Frequency-stabilized diode laser with the zeeman shift in an atomic vapor. *Applied Optics*, 37(15):3925, May 1998.

[6] J. Dalibard and C. Cohen-Tannoudji. Dressed-atom approach to atomic motion in laser light: the dipole force revisited. *Journal of the Optical Society of America B*, 2:1707, November 1987.

[7] J. Dalibard and C. Cohen-Tannoudji. Laser cooling below the doppler limit by polarization gradients: simple theoretical models. *Journal of the Optical Society of America B*, 6(11), November 1989.

[8] Ken Dutton, Steve Thompson, and Bill Barraclough. *The Art of Control Engineering.* Addison-Wesley, 1997.

[9] R. Grimm, M. Weidmuller, and Y. Ovchinnikov. Optical dipole traps for neutral atoms. *Advances in Atomic Molecular and Optical Physics*, 42:95–170, 2000.

[10] M. Key, I G. Hughes, W. Rooijakkers, B.E. Sauer, E.A. Hinds, D.J. Richardson, and P.G. Kazansky. Propagation of cold atoms along a miniature magnetic guide. *Physical Review Letters*, 84(7), February 2000.

[11] H.J. Metcalf and P. Van der Straten. *Laser Cooling and Trapping.* Graduate Texts in Contemporary Physics. Springer-Verlag, 1999.

[12] T. Petelski, M. Fattori, G. Lamporesi, J. Stuhler, and G.M. Tino. Doppler-free spectroscopy using magnetically induced dichroism of atomic vapor: a new scheme for laser frequency locking. *European Physical Journal D*, December 2002.

[13] W. D. Phillips. Laser cooling and trapping of neutral atoms. In *Proceedings of the International School of Physics*, July 1991.

[14] E. L. Raab, M. Prentiss, Alex Cable, Steven Chu, and D. E. Pritchard. Trapping of neutral sodium atoms with radiation pressure. *Physics Review Letters*, 59(23):2631–2634, December 1987.

[15] Daniel A. Steck. Rubidium 87 d2 line data. Available at http://steck.us/alkalidata, October 2003.

[16] P. J. Ungar, D.S. Weiss, E. Riis, and Steven Chu. Optical molasses and multilevel atoms: theory. *Journal of the Optical Society of America B*, 6(11), November 1989.

[17] G. Wasik, W. Gawlik, J. Zachorowski, and W. Zawadzki. Laser frequency stabilization by dopple-free magnetic dichroism. *Applied Physics B*, 75(1), 2002.

[18] I. Yavin, M. Weel, A. Andreyuk, and A. Kumarakrishnan. A calculation of the time-of-flight distribution of trapped atoms. *American Journal of Physics*, 70(3), 2002.